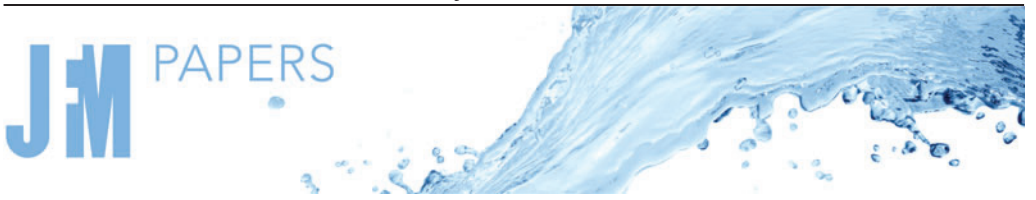
J. Fluid Mech. (2022), *vol*. 939, A17, doi:10.1017/jfm.2022.114



Exponential asymptotics for steady parasitic capillary ripples on steep gravity waves

Josh Shelton[1],† **and Philippe H. Trinh**[1],†

[1]Department of Mathematical Sciences, University of Bath, Bath BA2 7AY, UK

(Received 10 July 2021; revised 28 November 2021; accepted 31 January 2022)

In this paper, we develop an asymptotic theory for steadily travelling gravity–capillary waves under the small-surface tension limit. In an accompanying work (Shelton *et al.*, *J. Fluid Mech.*, vol. 922, 2021) it was demonstrated that solutions associated with a perturbation about a leading-order gravity wave (a Stokes wave) contain surface-tension-driven parasitic ripples with an exponentially small amplitude. Thus, a naive Poincaré expansion is insufficient for their description. Here, we develop specialised methodologies in exponential asymptotics for derivation of the parasitic ripples on periodic domains. The ripples are shown to arise in conjunction with Stokes lines and the Stokes phenomenon. The resultant analysis associates the production of parasitic ripples to the complex-valued singularities associated with the crest of a steep Stokes wave. A solvability condition is derived, showing that solutions of this type do not exist at certain values of the Bond number. The asymptotic results are compared with full numerical solutions and show excellent agreement. The work provides corrections and insight of a seminal theory on parasitic capillary waves first proposed by Longuet-Higgins (*J. Fluid Mech.*, vol. 16, issue 1, 1963, pp. 138–159).

Key words: capillary flows, surface gravity waves

1. Introduction

Consider the situation of a steep gravity-driven Stokes wave: a two-dimensional periodic surface wave of an inviscid and irrotational fluid travelling without change of shape or form. If a small amount of surface tension is included, it is reasonable to expect that, under certain conditions, the profile of the Stokes wave is modified or perturbed by a small amount. Physically, such perturbations may manifest as small-amplitude capillary-driven ripples concentrated near the crest of the wave. We refer to these perturbations as parasitic ripples, an experimental observation of which appears in figure 1.

† Email addresses for correspondence: j.shelton@bath.ac.uk, p.trinh@bath.ac.uk

© The Author(s), 2022. Published by Cambridge University Press

https://doi.org/10.1017/jfm.2022.114 Published online by Cambridge University Press

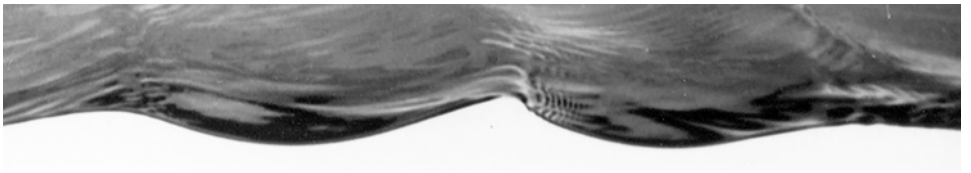


Figure 1. Experimental picture showing parasitic ripples located near the crests of a steep gravity-dominated wave. Note that the ripples appear in an asymmetric manner; mechanisms that produce asymmetry are discussed in § 9.2. Image used with permission from Professor N. Ebuchi (Hokkaido University).

The purpose of this work is to develop a precise asymptotic theory for the parasitic ripples that arise in the permanently progressive framework of a travelling water wave. In particular, we demonstrate that for small surface tension, the parasitic ripples are described by an exponentially small remainder to the base water wave, which is given by a typical asymptotic expansion in algebraic powers of the surface tension parameter. Their description requires the use of exponential asymptotics and, indeed, it is this requirement that distinguishes this work from the previous analytical treatments.

1.1. *Steady parasitic solutions for small surface tension*

Here, we provide a brief overview of how our treatment differs from previous works. To begin, the water-wave problem can be formulated in terms of an unknown streamline speed, q, and streamline angle, θ, considered as functions of the velocity potential, ϕ, over the periodic domain $-\frac{1}{2} < \phi \leqslant \frac{1}{2}$. The free surface is then governed by Bernoulli's equation,

$$F^2 q^2 \frac{\mathrm{d}q}{\mathrm{d}\phi} + \sin(\theta) - Bq\frac{\mathrm{d}}{\mathrm{d}\phi}\left(q\frac{\mathrm{d}\theta}{\mathrm{d}\phi}\right) = 0, \tag{1.1}$$

where F is the Froude number and B is the (inverse) Bond number. These non-dimensional constants are given by

$$F = \frac{c}{\sqrt{g\lambda}} \quad \text{and} \quad B = \frac{\sigma}{\rho g \lambda^2}, \tag{1.2a,b}$$

where c is the wave speed, g is the constant acceleration due to gravity, λ is the wavelength, ρ is the fluid density and σ is the coefficient of surface tension. The limit of small-surface tension is given by $B \to 0$. A list of variables, parameters and notation used in the main text is provided in table 1.

As it turns out, the structure of the solution space for the free-surface gravity–capillary wave problem is remarkably sophisticated. Recently, a portion of this solution space was investigated numerically by Shelton, Milewski & Trinh (2021) for fixed energy, with a focus on determining the small-surface tension limit of $B \to 0$. Multiple branches of solutions were found, each of which can be indexed by the number of capillary-driven ripples that appear in the periodic domain. This solution space is shown in figure 2 and the structure of 'fingers' (as introduced in the previous work) can be observed.

Two different asymptotic limits are visible in these solutions. The first limit is observed from the solutions in figures 2(*d*)–2(*f*) at the lower parts of each of the fingers, which are highly oscillatory with some modulation across the domain. In this region, the solution

https://doi.org/10.1017/jfm.2022.114 Published online by Cambridge University Press

	Symbol	Notes
Dimensional quantities	c	Wave speed
	g	Constant acceleration due to gravity
	ρ	Fluid density
	λ	Wavelength
	σ	Constant coefficient of surface tension
Parameters	q	Streamline speed
	θ	Streamline angle
	$\phi + \mathrm{i}\psi$	Complex potential comprised of velocity potential ϕ and streamfunction ψ
	f	Complex valued domain, relabeled from the analytically continued velocity potential ϕ_c
	a	Direction of analytic continuation, where $a = \pm 1$
	$\mathscr{E}$	Energy
	B	Bond number
	F	Froude number
Subscript notation	x_ϕ	Partial derivative of x with respect to ϕ
	q_n	nth order of the asymptotic series $\sum_{n=0}^{\infty} B^n q_n$
	E_{hw}	Text, used for hw (highest wave), homog (homogeneous) and phys (physical)
	Q_a	Direction of analytic continuation of the free-surface solution, $Q(f)$
Further notation	$\hat{\mathscr{H}}$	Complex-valued Hilbert transform
	f^*	Location of the principal singularity of the analytically continued Stokes wave
	$\bar{q}$	Overbar, denoting the remainder to a truncated asymptotic series
	$\mathfrak{q}$	Frankerscript, denoting the combined solution $q\|_{a=-1} + q\|_{a=1}$
	ξ	Forcing terms which appear in the equation for the remainder, $\bar{q}$
	$\hat{q}$	Hats denote an inner asymptotic solution within a boundary layer associated with the singularity at $f = af^*$

Table 1. List of variables, parameters and notation used in the main text.

can be approximated by a multiple-scales framework, with

$$q(\phi) = \sum_{n=0}^{\infty} B^n q_n(\phi, \hat{\phi}), \tag{1.3}$$

where $\hat{\phi} = \phi/B$ is the fast scale. Substitution of this ansatz into Bernoulli's equation (1.1) yields, at order $1/B$, the pure-capillary equation of Crapper (1957) for the small-scale ripples

$$F_0^2 q_0^2 \frac{\partial q_0}{\partial \hat{\phi}} - q_0 \frac{\partial}{\partial \hat{\phi}} \left(q_0 \frac{\partial \theta_0}{\partial \hat{\phi}} \right) = 0. \tag{1.4}$$

Thus, for these multiple-scale solutions, the highly oscillatory parasitic ripples appear in the leading-order term, $q_0(\phi, \hat{\phi})$, of the expansion. We will focus on this asymptotic regime in future work.

The second asymptotic limit can be observed in figures 2(*a*)–(*c*). As these solutions approach the pure-gravity (Stokes) solution with the same fixed value of the energy as

https://doi.org/10.1017/jfm.2022.114 Published online by Cambridge University Press

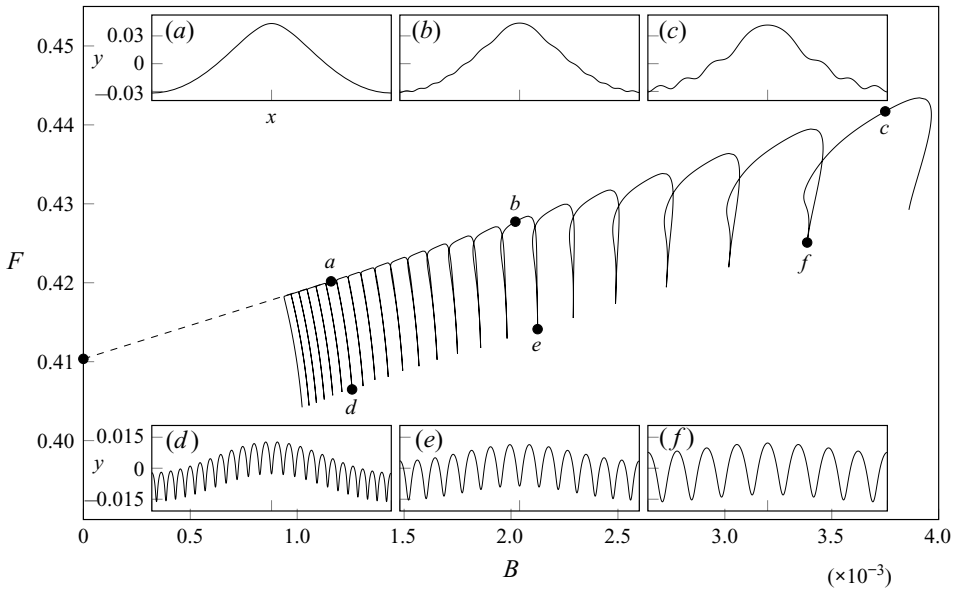


Figure 2. The numerical (B, F) solution space calculated by Shelton *et al.* (2021) is shown for a fixed energy of $\mathscr{E} = 0.3804$. Insets (a)–(c) show the physical free surface for those cases corresponding to exponentially small parasitic ripples on Stokes waves; insets (d)–(f) show a different multiple-scales regime.

$B \to 0$, the leading order solution q_0 contains no ripples. Moreover, a standard perturbative series of the form

$$q(\phi) = \sum_{n=0}^{\infty} B^n q_n(\phi) \tag{1.5}$$

will also not contain the parasitic ripples observed in the numerical solutions. This is due to the exponential smallness of the amplitude of these ripples, which was confirmed numerically by Shelton *et al.* (2021) and is shown to form a straight line in the semi-log plot in figure 3.

Thus, in the $B \to 0$ limit, the capillary-driven ripples exhibit different behaviours according to two distinct asymptotic limits of:

(i) a multiple-scales solution, for which the ripples appear in the leading-order approximation of the solution; and
(ii) a standard perturbative series about a Stokes wave, for which the parasitic ripples appear beyond all orders.

It is this latter asymptotic regime that we focus on in this work.

In the context of the second scenario, an early analytical theory for the generation of these parasitic ripples was proposed by Longuet-Higgins (1963), who considered a small surface-tension perturbation about a base Stokes wave. Although Longuet-Higgins' seminal work provides a crucial basis for our analysis in this paper, we also demonstrate that there are a number of key asymptotic inconsistencies that appear in the historical 1963 work. These inconsistencies turn out to be connected with modern understanding of exponential asymptotics (Berry 1989; Olde Daalhuis *et al.* 1995; Chapman, King & Adams 1998), and may have led to the poor agreement noted by Perlin, Lin & Ting

https://doi.org/10.1017/jfm.2022.114 Published online by Cambridge University Press

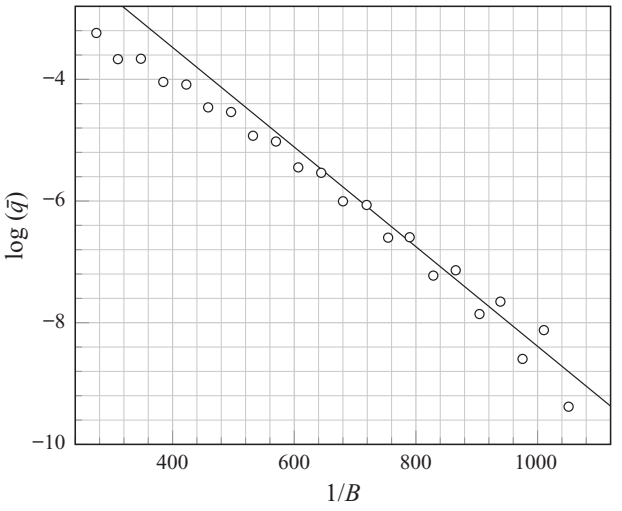


Figure 3. Our analytical prediction of the exponential-scaling of the parasitic ripple magnitude, $\bar{q}$, (line) is compared with numerical results of the full nonlinear equations (circles). These results have both been calculated with an energy of $\mathscr{E} = 0.3804$ and the gradient of the analytical result is -0.0082.

(1993) in comparison with numerical solutions of the full nonlinear problem. One of the primary objectives of our work is to provide a critical re-examination of the seminal Longuet-Higgins (1963) paper, which we perform in § 3. Note that we provide a more complete literature review of theories and research on the parasitic capillary problem in our discussion of § 9.

As we demonstrate, the intricate difficulties involved in formulating a corrected theory for the $B \to 0$ limit are linked to the presence of singularities in the analytical continuation of the leading-order gravity-wave solution. Due to the singularly perturbed nature of Bernoulli's equation (1.1), successive terms in the asymptotic expansion of the solution require repeated differentiation of the singularity in the leading-order solution. This causes the expansion to diverge. In studying this divergence, a form for the exponentially small correction terms to the asymptotic series is found by truncating the series optimally and these corrections correspond to the anticipated parasitic ripples.

1.2. *Outline of the paper*

We begin in § 2 with the mathematical formulation of the non-dimensional gravity–capillary wave system, which is analytically continued into the complex potential plane. In § 3 we provide a detailed overview of the Longuet-Higgins (1963) analytical methodology. In § 4, we consider a perturbation expansion for small values of the surface tension, B. Subsequent terms in this expansion rely on differentiation of the leading-order gravity-wave solution. Thus, singularities in the analytic continuation of the free-surface gravity-wave produce a divergence in the asymptotic series as further terms are considered. The scaling of the principal upper-half and lower-half singularities are derived in § 5. The divergence of the late terms of the asymptotic expansion is then considered in § 6. This allows us to find the Stokes lines for our problem, which are shown in § 7 to produce the switching of exponentially small terms of the solution via Stokes phenomenon. Application of the periodicity conditions then yields an analytical solution for these parasitic ripples and an accompanying solvability condition. These solutions and the

https://doi.org/10.1017/jfm.2022.114 Published online by Cambridge University Press

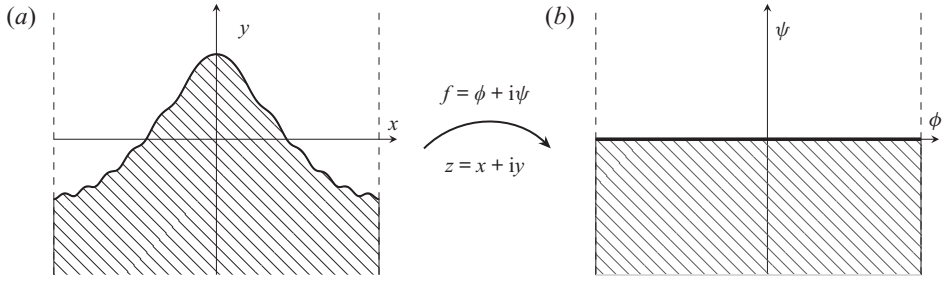


Figure 4. The conformal map from (*a*) the physical $z = x + \mathrm{i}y$-plane to (*b*) the complex $f = \phi + \mathrm{i}\psi$-plane. The boundary, $y = \eta(x)$, is mapped to the line $\psi = 0$.

solvability condition are then compared with numerical solutions of the full nonlinear equations in § 8. Our findings are summarised in § 10, and discussion of further work occurs in § 9.

2. Mathematical formulation

We begin by considering the two-dimensional free-surface flow of an inviscid, irrotational and incompressible fluid of infinite depth. The effects of gravity and surface tension are included. We assume the free surface to be periodic with wavelength λ, and it is chosen to move to the right with wave speed c. Imposing a sub-flow within the fluid in the opposite direction cancels out the lateral movement; this results in a steady free surface when $\partial_t = 0$, now assumed to be located at $y = \eta(x)$. A typical configuration is shown in figure 4. The system is non-dimensionalised using λ and c for the units of length and velocity, respectively, and the set of governing equations is taken to be the same as those considered by Shelton *et al.* (2021):

$$\phi_{xx} + \phi_{yy} = 0 \quad \text{for } y \leqslant \eta, \tag{2.1a}$$

$$\phi_y = \eta_x \phi_x \quad \text{at } y = \eta, \tag{2.1b}$$

$$\frac{F^2}{2}(\phi_x^2 + \phi_y^2) + y - B\frac{\eta_{xx}}{(1+\eta_x^2)^{3/2}} = \frac{F^2}{2} \quad \text{at } y = \eta, \tag{2.1c}$$

$$\phi_y \to 0 \quad \text{and} \quad \phi_x \to -1 \quad \text{as } y \to -\infty. \tag{2.1d}$$

Thus, the flow is governed by Laplace's equation (2.1*a*), kinematic and dynamic boundary conditions in (2.1*b*) and (2.1*c*), respectively, at the free surface, and the deep-water condition (2.1*d*). The constants F and B are the Froude and Bond numbers, introduced earlier in (1.2*a*,*b*). Periodicity of the flow and wave profile is specified by enforcing

$$\nabla\phi\left(x - \tfrac{1}{2}, y\right) = \nabla\phi\left(x + \tfrac{1}{2}, y\right) \quad \text{and} \quad \eta\left(x - \tfrac{1}{2}\right) = \eta\left(x + \tfrac{1}{2}\right). \tag{2.1e}$$

In addition to the governing equations in (2.1), we also enforce an amplitude parameter as a measure of nonlinearity of the solution. This is derived from the physical bulk energy of the wave via Appendix A of Shelton *et al.* (2021). This yields

$$\mathscr{E} = \frac{1}{E_{hw}}\int_{-1/2}^{1/2}\left[\frac{F^2}{2}y(x_\phi - 1) + B\left(\sqrt{(x_\phi^2 + y_\phi^2)} - x_\phi\right) + \frac{1}{2}y^2 x_\phi\right]\mathrm{d}\phi, \tag{2.2}$$

where the three groupings of terms correspond to the kinetic, capillary and gravitational potential energies. In (2.2), we have rescaled with the energy of the limiting classical

https://doi.org/10.1017/jfm.2022.114 Published online by Cambridge University Press

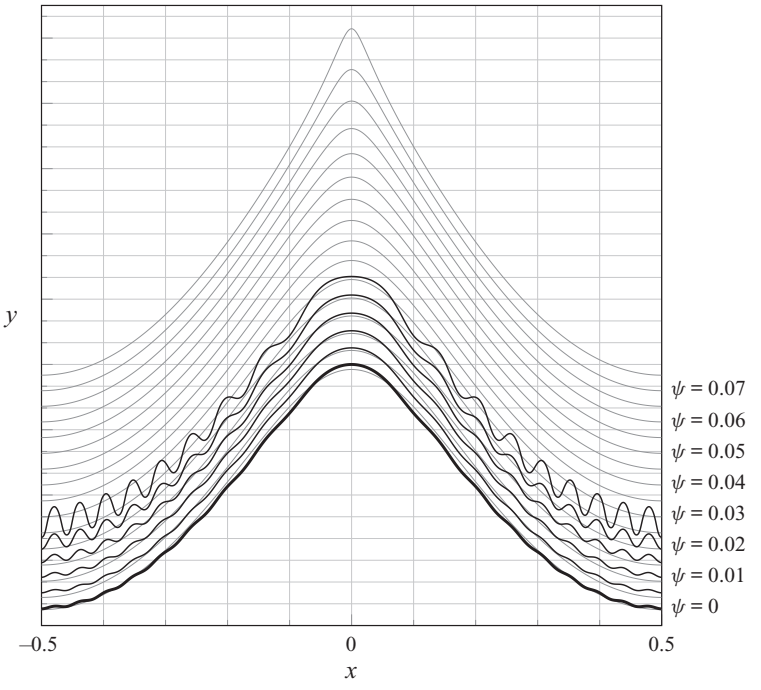


Figure 5. The analytic continuation into the upper-half plane is calculated numerically for two solutions of (2.1) with $\psi = 0$. The first is a gravity wave with $B = 0$, $F = 0.4104$ and $\mathscr{E} = 0.3804$ (thin grey lines) and the second a gravity–capillary wave with $B = 0.001$, $F = 0.4188$ and $\mathscr{E} = 0.3804$ (bold lines). The solutions with $\psi > 0$ satisfy the analytically continued equations (2.9) and Re[x] versus Re[y] is shown. This image can be compared with figure 11 of Longuet-Higgins & Fox (1978), which provides a streamline plot of the pure-gravity solution in the analytically continued plane.

Stokes wave, $E_{hw} \approx 0.00184$. A central idea in Shelton *et al.* (2021) concerned the importance of choosing an amplitude condition on the water waves, and we refer readers to § 2.2 of that work for further discussion.

Finally, based on the previous study in Shelton *et al.* (2021), we note that once the energy condition (2.2) is imposed, there is only a single degree of freedom in specifying either F or B. We typically consider the Bond number as a free parameter, which results in the Froude number as an eigenvalue that must be determined via the system (2.1).

2.1. *The* (q, θ) *formulation*

In this section, we repose the two-dimensional governing system (2.1) as a one-dimensional boundary-integral formulation in terms of the free-surface speed and angle. Following the traditional treatment of potential free-surface flows, we introduce the complex potential $f = \phi + \mathrm{i}\psi$. Rather than consider $f = f(z)$, we instead consider $z = z(f)$ and, hence, the flow region is known in the potential plane. The complex potential plane is shown in figure 4. From this definition, the complex velocity can be found to be $\mathrm{d}f/\mathrm{d}z = u - \mathrm{i}v$, where (u, v) are the horizontal and vertical velocities.

Introducing q as the streamline speed and θ as the streamline angle by the relationship $q\mathrm{e}^{-\mathrm{i}\theta} = u - \mathrm{i}v$ then yields

$$\frac{\mathrm{d}f}{\mathrm{d}z} = q\mathrm{e}^{-\mathrm{i}\theta}. \tag{2.3}$$

https://doi.org/10.1017/jfm.2022.114 Published online by Cambridge University Press

In this form, Bernoulli's equation (2.1*c*) is written as

$$F^2q^2\frac{\mathrm{d}q}{\mathrm{d}\phi}+\sin(\theta)-Bq\frac{\mathrm{d}}{\mathrm{d}\phi}\left(q\frac{\mathrm{d}\theta}{\mathrm{d}\phi}\right)=0. \tag{2.4a}$$

By the analyticity of $\log q-\mathrm{i}\theta$, we introduce the boundary-integral equation which relates q to the Hilbert transform of θ operating over the free surface. For our periodic domain from $-1/2$ to $1/2$, we integrate $\log q-\mathrm{i}\theta$ using Cauchy's theorem and use the periodicity conditions

$$q\left(\phi-\tfrac{1}{2}\right)=q\left(\phi+\tfrac{1}{2}\right)\quad\text{and}\quad\theta\left(\phi-\tfrac{1}{2}\right)=\theta\left(\phi+\tfrac{1}{2}\right), \tag{2.4b}$$

which follow from (2.1*e*), and the deep-water conditions (2.1*d*) to derive the periodic Hilbert transform given by

$$\log(q)=\mathscr{H}[\theta](\phi)=\fint_{-1/2}^{1/2}\theta(\phi')\cot[\pi(\phi'-\phi)]\mathrm{d}\phi'. \tag{2.4c}$$

In the above, $\fint$ is the Cauchy principal-value integral. The above provides the crucial relationship between the components q and θ, and further details on the derivation of the boundary-integral relations can be found in chapter 6 of Vanden-Broeck (2010).

Finally, the energy expression (2.2) is also considered in terms of (q,θ). Noting that $x_\phi=q^{-1}\cos(\theta)$ and $y_\phi=q^{-1}\sin\theta$, we substitute $y=(F^2/2)(1-q^2)+Bq\theta_\phi$ from Bernoulli's equation to find

$$\mathscr{E}=\frac{1}{E_{hw}}\int_{-1/2}^{1/2}\Big[\mathcal{G}_0(\phi)+B\mathcal{G}_1(\phi)+B^2\mathcal{G}_2(\phi)\Big]\mathrm{d}\phi, \tag{2.4d}$$

where we have defined components

$$\left.\begin{aligned}\mathcal{G}_0(\phi)&=\frac{F^4}{8q}(1-q^2)(3\cos\theta-2q-q^2\cos\theta),\\ \mathcal{G}_1(\phi)&=\frac{(1-\cos\theta)}{q}+\frac{F^2\theta_\phi}{2}(2\cos\theta-q-q^2\cos\theta),\\ \mathcal{G}_2(\phi)&=\frac{q\theta_\phi^2\cos\theta}{2}.\end{aligned}\right\} \tag{2.5}$$

In summary, the water-wave problem, as formulated for q and θ, involves the solution of (2.4*a*)–(2.4*d*). Note that the above sets of equations all involve the evaluation of q and θ on the streamline $\psi=0$.

2.2. *Analytic continuation*

As we show, the exponential asymptotics procedure of § 7 requires the continuation of the free-surface solutions, $q(\phi+0\mathrm{i})$ and $\theta(\phi+0\mathrm{i})$, into the complex plane, where $\phi\in\mathbb{C}$. This free-surface continuation procedure is depicted in figure 6. Hence, we analytically continue Bernoulli's equation (2.4*a*) and the boundary-integral equation (2.4*c*) into the complex ϕ-plane. The independent variable ϕ is complexified by considering $\phi\mapsto\phi_c\in\mathbb{C}$ and, hence, q and θ are analytically continued. For convenience, we relabel ϕ_c as f. Thus, Bernoulli's equation remains in an identical form to (2.4*a*), but with the variable ϕ replaced by f.

https://doi.org/10.1017/jfm.2022.114 Published online by Cambridge University Press

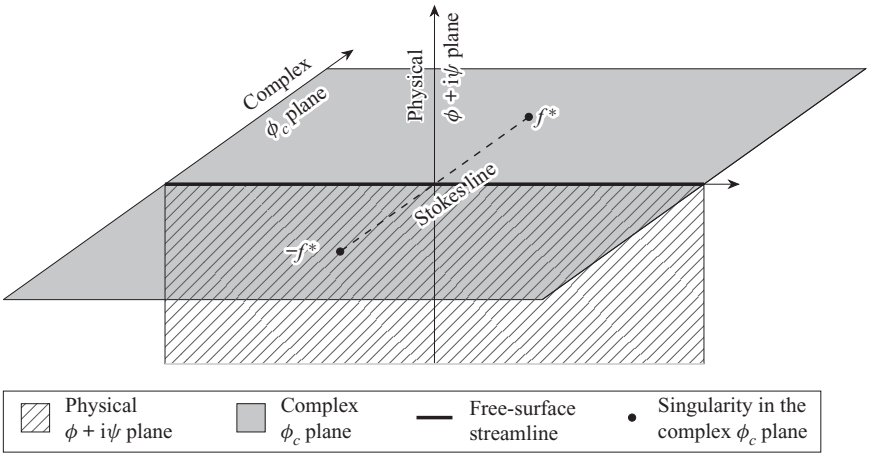


Figure 6. A schematic of our analytic continuation procedure demonstrates the difference between the physical $\phi + i\psi$ plane and our complexified ϕ_c space. The location of the principle upper- and lower-half singularities at f^* and $-f^*$ of the leading-order flow field are shown by circles, and the main Stokes line from § 7 is shown dashed.

For the boundary-integral equation (2.4*c*), we must consider the complexification of the Hilbert transform. Let us write

$$\mathscr{H}[\theta] = \hat{\mathscr{H}}[\theta] - ai\theta, \tag{2.6}$$

where $\hat{\mathscr{H}}[\theta]$ is the complex-valued Hilbert transform,

$$\hat{\mathscr{H}}[\theta](f) = \int_{-1/2}^{1/2} \theta(\phi') \cot\left[\pi(\phi' - f)\right] \mathrm{d}\phi'. \tag{2.7}$$

Note that the integral above is only evaluated along the physical free surface, parameterised in terms of ϕ', where θ takes real values.

In (2.6), we have also introduced the parameter, a, which is defined by

$$a = \begin{cases} +1 & \text{for } \mathrm{Im}(f) > 0, \\ -1 & \text{for } \mathrm{Im}(f) < 0. \end{cases} \tag{2.8}$$

When the Hilbert transform relationship is extended into the upper-half-f-plane, $a = 1$, whereas $a = -1$ for continuation into the lower-half-f-plane. The validity of (2.6) as a legitimate complexification of the Hilbert transform is verified by taking $\mathrm{Im}(f) \to 0$ on the right-hand side. Then $\hat{\mathscr{H}}[\theta]$ yields a principal value integral and residue. The residue contribution changes sign between $\mathrm{Im}(f) \to 0^+$ and $\mathrm{Im}(f) \to 0^-$, yielding the constant a.

In summary, the governing equations for the analytically continued q and θ values are given by

$$F^2 q^2 q' + \sin(\theta) - Bq(q\theta')' = 0, \tag{2.9a}$$

$$\log(q) + ai\theta = \hat{\mathscr{H}}[\theta], \tag{2.9b}$$

$$\mathscr{E} = \frac{1}{E_{hw}} \int_{-1/2}^{1/2} \left[\mathcal{G}_0(\phi) + B\mathcal{G}_1(\phi) + B^2\mathcal{G}_2(\phi)\right] \mathrm{d}\phi, \tag{2.9c}$$

$$q\left(-\tfrac{1}{2}\right) = q\left(\tfrac{1}{2}\right) \quad \text{and} \quad q'\left(-\tfrac{1}{2}\right) = q'\left(\tfrac{1}{2}\right). \tag{2.9d}$$

https://doi.org/10.1017/jfm.2022.114 Published online by Cambridge University Press

Note that although (2.9*a*) and (2.9*b*) are evaluated through complex f-space, the energy condition is most easily evaluated on the physical free surface. Here and henceforth, we use primes ($'$) to denote differentiation in f. This system will be solved in § 4 with an expansion holding under the limit of $B \to 0$.

3. A critical examination of the Longuet-Higgins (1963) theory

Longuet-Higgins (1963) proposed a theory for the generation of steady parasitic ripples by considering an asymptotic expansion for small surface tension such that a gravity wave was obtained at leading order. In § 3 he wrote the following perturbative form for the solutions,

$$q(\phi, \psi) = q_0 + \bar{q}, \quad \theta(\phi, \psi) = \theta_0 + \bar{\theta}, \quad y(\phi, \psi) = y_0 + \bar{y}, \tag{3.1a–c}$$

with y denoting the wave height. All quantities are dimensional and functions of the potential, ϕ, and stream function, ψ. Let us introduce the logarithm of the speed by $\tau = \log(q/c)$, where c is the wave speed. In writing $\tau = \tau_0 + \bar{\tau}$, this yields $q_0 = c\mathrm{e}^{\tau_0}$ and $\bar{q} = q_0\bar{\tau}$ for $\bar{\tau}$ assumed small.

The expression that Longuet-Higgins produced for the capillary ripples was [cf. equation (5.18) in Longuet-Higgins 1963]

$$\bar{\tau} - \mathrm{i}\bar{\theta} \sim F(\phi)\exp(-\mathrm{i}c\alpha(\phi)/T') \quad \text{for } \phi > 0, \tag{3.2a}$$

where the functional prefactor, $F(\phi)$, and exponent, $\alpha(\phi)$, are given by

$$F(\phi) = 4\mathrm{i}\exp\left(\mathrm{i}\int_0^{\phi}\frac{\partial\tau_0}{\partial\psi}\mathrm{d}\phi\right)\int_0^{\infty}\left(\frac{\partial\tau_0}{\partial\psi}\cos(\alpha c/T')\right)\mathrm{d}\phi, \tag{3.2b}$$

$$\alpha(\phi) = \int_0^{\phi}\mathrm{e}^{\tau_0}\,\mathrm{d}\phi. \tag{3.2c}$$

Here, T' is the dimensional surface tension coefficient, assumed to be small. Note that $\alpha(\phi)$ involves integration of a real-valued e^{τ_0} over real-valued ϕ and, hence, α is also real.

One of the main contributions of our work is to provide an improvement on the above formulae, which contains a number of problems related to the capture of small ripples. The three most important issues are as follows.

(i) The functional form of the prefactor, $F(\phi)$, in (3.2*c*) is incorrect; the form written above emerges as a consequence of certain asymptotic inconsistencies in the derivation.

(ii) Longuet-Higgins predicted correctly that the capillary ripples would exhibit wavelengths scaling with T', but in closer examination of (3.2*a*), the expression predicts a wave amplitude that is of $O(1)$ and independent of T'. We find that for small values of the surface tension, the wave amplitude is exponentially small in T' (indeed this should be clear from figure 3).

(iii) The above formulation does not provide any restriction on the solution space (i.e. the existence of a solvability condition observed in the full numerical simulations). It particular, it does not capture any of the observed bifurcation structure seen in figure 2.

Note that a portion of the work of Longuet-Higgins (1963) is devoted to studying the addition of viscosity and also incorporating the almost-highest wave theory of Longuet-Higgins & Fox (1977) into (3.2). However, in the present authors' view, the

https://doi.org/10.1017/jfm.2022.114 Published online by Cambridge University Press

treatment following § 6 of the 1963 work becomes increasingly *ad hoc* and difficult to analyse in view of the fundamental issues with (3.2).

We now discuss these key issues (i)–(iii) in detail.

3.1. *Asymptotic inconsistencies in Longuet-Higgins (1963)*

Numerical evidence was provided by Shelton *et al.* (2021) (see figure 3) to demonstrate that, for those solutions exhibiting small-scale ripples on an underlying gravity wave, the amplitude of these parasitic ripples is exponentially small as $T' \to 0$. Solutions that display such exponentially small behaviour cannot be described purely by a typical Poincaré expansion which contains only algebraic powers of the small parameter; their description will instead appear beyond all orders of the standard Poincaré expansion.

We now review Longuet-Higgins' approach in our non-dimensional formulation (using the Bond number, B, and Froude number, F, in (1.2*a*,*b*) instead of T' and c). We start with the integrated form of Bernoulli's equation from (1.1) given in terms of y and the streamline speed, q, as

$$\frac{F^2}{2}q^2 + y - B\frac{\partial q}{\partial \psi} = \text{const.}, \tag{3.3}$$

where the derivative in the ψ direction can be converted into a derivative the ϕ direction via the Cauchy–Riemann equations. In his §3, Longuet-Higgins considered a perturbation $(\bar{y}, \bar{q})$ about the gravity-wave (y_0, q_0) with the truncations from (3.1*a–c*) to find

$$\frac{F^2}{2}(q_0^2 + 2q_0\bar{q} + \bar{q}^2) + (y_0 + \bar{y}) - B\left(\frac{\partial q_0}{\partial \psi} + \frac{\partial \bar{q}}{\partial \psi}\right) = \text{const.} \tag{3.4}$$

Here, the $O(1)$ terms, $F^2q_0^2/2 + y_0 = \text{const.}$, are satisfied exactly as this is the gravity-wave equation with solutions (y_0, q_0). Thus, we obtain

$$\underbrace{F^2q_0\bar{q} + \bar{y} - B\frac{\partial q_0}{\partial \psi}}_{O(B)} - \underbrace{B\frac{\partial \bar{q}}{\partial \psi}}_{O(B^2)} = \underbrace{-\frac{F^2\bar{q}^2}{2}}_{O(B^2)}. \tag{3.5}$$

The asymptotic behaviour indicated by the under-braced quantities follows by making the standard assumption that the leading corrections, $\bar{y}$ and $\bar{q}$, are both of $O(B)$. Consequently, $\bar{q} \ll q_0$, and so Longuet-Higgins neglected the nonlinear term $\bar{q}^2$ on the right-hand side of this equation. However, the $O(B^2)$ term on the left-hand side was not neglected. This assumption, which appears in his (5.1), is asymptotically inconsistent. In fact, this inconsistency is how Longuet-Higgins was able to produce approximations to an *a priori* exponentially small capillary ripple, because, otherwise, all corrections are ripple-free and algebraic in B.

The above asymptotic inconsistency is somewhat typical in early models of many exponential asymptotic problems. There are two (formally correct) methods to proceed with (3.5).

(i) We may correctly treat $\bar{y}$ and $\bar{q}$ to both be of $O(B)$. The leading-order terms in (3.5) are, thus,

$$F^2q_0\bar{q} + \bar{y} - B\frac{\partial q_0}{\partial \psi} = 0, \tag{3.6}$$

and would yield the $O(B)$ capillary correction term. The procedure could be continued to quadratic orders of B and higher, but the resultant perturbative solution

https://doi.org/10.1017/jfm.2022.114 Published online by Cambridge University Press

would never yield an exponentially small ripple. In essence, this is a derivation of the regular perturbative expansion and leads to the analysis of § 4.

(ii) Alternatively, we may consider $\bar{y}$ and $\bar{q}$ to both scale as $\sim \mathrm{e}^{-\alpha/B}$, i.e. for solutions to be of Wentzel–Kramers–Brillouin–Jeffreys (WKBJ) type. As differentiation of this ansatz yields a factor of $1/B$, the dominant terms in (3.5) change to

$$\underbrace{F^2 q_0 \bar{q} - B\frac{\partial \bar{q}}{\partial \psi}}_{O(\mathrm{e}^{-\alpha/B})} = \underbrace{B q_0'}_{O(B)}. \tag{3.7}$$

The form of the above equation would allow for the correct prediction of the WKBJ phase, α, but not the correct prefactor (amplitude); this is on account of the fact the right-hand side is the result of a one-term truncation of the Poincaré expansion (3.1*a–c*). Instead, the correct procedure must involve additional terms of the regular expansion. In general, the right-hand side is of $O(B^N)$ with $N \to \infty$ as $B \to 0$. In order to derive the exponentially small ripples, we must optimally truncate with N chosen carefully (Chapman *et al.* 1998).

Longuet-Higgins had worked with the asymptotically inconsistent (3.5), with the right-hand side set to zero, and this was used to derive the solution (3.2).

As shown in § 7.3, the ripples have the analytical behaviour

$$q_{exp}(\phi) = \Lambda \mathcal{F}(\phi) \exp\left(-\frac{\chi(\phi)}{B}\right), \tag{3.8}$$

where Λ is a constant coefficient, $\mathcal{F}(\phi)$ is a functional prefactor and $\chi(\phi)$ is the exponentially small dependence of the solution, which is related to the quantity $\alpha(\phi)$. These components will be significantly different than those derived by Longuet-Higgins in (3.2). In order to be correct, the above expression must be derived through optimal truncation of the standard asymptotic expansion, rather than using the one-term truncation in (3.1*a–c*).

We note that it is still nevertheless possible to capture exponentially small behaviour with the truncation (3.1*a–c*) used by Longuet-Higgins. A comprehensive review of truncations of this type, for the case of free-surface flows, was given by Trinh (2017) who, aided by the use of exponential asymptotics, discussed how the functional form of the exponentially small waves changes when different truncations are made. The type utilised here by Longuet-Higgins in (3.1*a–c*) is an $N = 1$ truncation as only one term of the asymptotic series is included. Although this truncation (if dealt with in an asymptotically consistent manner) can predict the correct exponentially small scaling of the solution, the functional form of the prefactor and its magnitude [cf. (3.2*b*)] will be incorrect.

3.2. *The choice of integration in the exponential argument*

We now discuss the second issue with Longuet-Higgins' analytical solution, which is that (3.2) predicts an $O(1)$ solution magnitude. For real values of ϕ, α takes purely real values. Thus, as his solution contains $\mathrm{e}^{-\mathrm{i}c\alpha/T'}$, only a rapidly oscillating waveform of wavelength $O(\epsilon)$ is predicted. The issue is not precisely related to the functional form of the exponential argument, because modulo the scalings, it can be confirmed via our

https://doi.org/10.1017/jfm.2022.114 Published online by Cambridge University Press

work that

$$-\frac{1}{B}\frac{\mathrm{d}\chi}{\mathrm{d}\phi} \propto -\frac{\mathrm{i}c}{T'}\frac{\mathrm{d}\alpha}{\mathrm{d}\phi}. \tag{3.9}$$

However, Longuet-Higgins restricts ϕ to take real values and forces the starting point of integration in $\alpha(\phi)$ to be at $\phi = 0$. This is later matched to an *ad hoc* simplification near the crest of the wave. This misses a fundamental step in the determination of the parasitic ripples because, as we show, their existence is intimately connected with the singularities of $\chi'(\phi)$ in the analytic continuation of the free surface. In order to correctly resolve the Stokes phenomenon in § 7, integration in our expression for χ must begin from such singularities, and results in a path of integration through the complex-valued domain. The final result produces a complex-valued q_{exp}, which is paired with a conjugate contribution to in order to produce a real-valued solution with both exponentially small phase and amplitude.

4. The expansion for small surface tension, B

In the limit of $B \to 0$, we consider the traditional series expansions for q and θ, given by

$$q = \sum_{n=0}^{\infty} B^n q_n \quad \text{and} \quad \theta = \sum_{n=0}^{\infty} B^n \theta_n. \tag{4.1a,b}$$

These expansions will satisfy both Bernoulli's equation (2.9*a*) and the boundary-integral equation (2.9*b*) to each order in B. As noted in the discussion following (2.4*d*), specifying B and enforcing the energy constraint requires that F be treated as an eigenvalue. Hence, we also consider an expansion of the Froude number by

$$F = \sum_{n=0}^{\infty} B^n F_n. \tag{4.1c}$$

At leading order in (2.9*a*), (2.9*b*) and (2.4*d*) this results in the gravity-wave equations

$$F_0^2 q_0^2 \frac{\mathrm{d}q_0}{\mathrm{d}f} + \sin(\theta_0) = 0, \tag{4.2a}$$

$$\log(q_0) + a\mathrm{i}\theta_0 = \hat{\mathscr{H}}[\theta_0], \tag{4.2b}$$

$$\mathscr{E} = \frac{1}{E_{hw}} \int_{-1/2}^{1/2} \frac{F_0^4}{8q_0}(1 - q_0^2)(3\cos\theta_0 - 2q_0 - q_0^2\cos\theta_0)\,\mathrm{d}\phi, \tag{4.2c}$$

where we remind the reader that $a = \pm 1$ via the choice of analytic continuation into the upper- or lower-half planes, respectively [cf. (2.8)]. Here, the Hilbert transform in (4.2*b*) acts on the free surface for which f is real. The energy, $\mathscr{E}$, is a specified $O(1)$ constant, which we take to be less than unity.

At $O(B)$, we have for Bernoulli's equation,

$$F_0^2 q_0^2 \frac{\mathrm{d}q_1}{\mathrm{d}f} + 2F_0^2 q_0 q_0' q_1 + 2F_0 F_1 q_0^2 q_0' + \theta_1 \cos\theta_0 - q_0\left(q_0\theta_0'\right)' = 0, \tag{4.3a}$$

for the boundary-integral equation,

$$\frac{q_1}{q_0} + a\mathrm{i}\theta_1 = \hat{\mathscr{H}}[\theta_1], \tag{4.3b}$$

https://doi.org/10.1017/jfm.2022.114 Published online by Cambridge University Press

and finally for the energy constraint,

$$0 = \int_{-1/2}^{1/2} \left[\frac{(1-\cos\theta_0)}{q_0} + \frac{F_0^2\theta_0'}{2}(2\cos\theta_0 - q_0 - q_0^2\cos\theta_0) \right.$$
$$+ (3\cos\theta_0 - 2q_0 - q_0^2\cos\theta_0)\left(\frac{F_0^3F_1(1-q_0^2)}{2q_0} - \frac{F_0^4q_1}{8q_0}(1+q_0^2)\right)$$
$$\left. + \frac{F_0^4(1-q_0^2)}{8q_0}(-3\theta_1\sin\theta_0 - 2q_1 + q_0^2\theta_1\sin\theta_0 - 2q_0q_1\cos\theta_0)\right]\mathrm{d}\phi. \tag{4.3c}$$

We now consider the $O(B^n)$ components of (2.9*a*) and (2.9*b*). The solutions of these, q_n, θ_n and F_n, are denoted the late terms of the asymptotic expansions (4.1*a*,*b*) and (4.1*c*). An important feature of these solutions is that they diverge as $n \to \infty$. This is a consequence of the singularities in the leading-order solutions, q_0 and θ_0, which are derived in § 5. Evidently, the $O(B^n)$ equations will contain an unbounded number of terms as $n \to \infty$. However, due to the divergent nature of the late terms, only a few of these terms will influence the leading-order solution as $n \to \infty$.

Starting with Bernoulli's equation (2.9*a*), we retain the two leading orders in n, yielding

$$\left[F_0^2\left(q_0^2q_n' + 2q_0q_1q_{n-1}' + 2q_0q_0'q_n + \dots\right) + 2F_0F_1q_0^2q_{n-1}' + 2F_0F_nq_0^2q_0' + \dots\right]$$
$$+ [\theta_n\cos\theta_0 + \dots] - \left[q_0^2\theta_{n-1}'' + 2q_0q_1\theta_{n-2}'' + q_0\theta_0'q_{n-1}' + q_0q_0'\theta_{n-1}' + \dots\right] = 0. \tag{4.4a}$$

At $O(B^n)$, we expand the logarithm in the boundary-integral equation (2.9*b*) in order to obtain

$$\frac{q_n}{q_0} - \frac{q_1q_{n-1}}{q_0^2} + \dots + a\mathrm{i}\theta_n = \hat{\mathscr{H}}[\theta_n]. \tag{4.4b}$$

5. On the singularities of the leading-order flow

A crucial element of the exponential asymptotics analysis relies upon the understanding that the series (4.1*a*,*b*) will diverge on account of singularities (such as poles or branch points) in the analytic continuation of q and θ. More specifically, we shall find that the leading-order solution, q_0, which corresponds to the pure Stokes gravity wave via (4.2), contains branch points in the complex plane. As the determination of each subsequent order generally relies upon differentiating the previous, the result is that the order of the singularity increases as $n \to \infty$. This is shown in § 6.

On the assumption that the leading-order Stokes wave possesses a singularity in the complex plane, previously Grant (1973) derived the local asymptotic behaviour using a dominant balance. That is, by considering the complex velocity $\mathrm{d}f/\mathrm{d}z$ from (2.3), he showed that near to a point $f^* \in \mathbb{C}$ directly 'above' the wave crest

$$\frac{\mathrm{d}f}{\mathrm{d}z} \sim (f - f^*)^{1/2}. \tag{5.1}$$

In the exponential asymptotics to follow, we require the singular behaviour of the individual components of q_0 and θ_0. This is derived in the following analysis, along with a discussion of the difference between Grant's singularity in $\mathrm{d}f/\mathrm{d}z$ and those of (q_0, θ_0).

https://doi.org/10.1017/jfm.2022.114 Published online by Cambridge University Press

5.1. *Singularities in the analytic continuation of q_0 and θ_0*

The singular scaling of q_0 and θ_0 is now considered. We let f^* denote the 'crest' singularity in the upper-half-f-plane. We leave the constant, a, unspecified and take the limit of $f \to af^*$. First, it can be verified *a posteriori* that as $f \to af^*$, $|\operatorname{Im}\theta_0| \to \infty$ and

$$\sin\theta_0 = \frac{1}{2\mathrm{i}}\left[\mathrm{e}^{\mathrm{i}\theta_0} - \mathrm{e}^{-\mathrm{i}\theta_0}\right] \sim \frac{a}{2\mathrm{i}}\mathrm{e}^{a\mathrm{i}\theta_0}. \tag{5.2}$$

We multiply Bernoulli's equation (4.2*a*) by q_0, and use the above scaling for $\sin\theta_0$ to find

$$F_0^2 q_0^3 \frac{\mathrm{d}q_0}{\mathrm{d}f} = -q_0\sin\theta_0 \sim -\frac{a}{2\mathrm{i}}q_0\mathrm{e}^{a\mathrm{i}\theta_0}. \tag{5.3}$$

However, in taking the exponential of the boundary-integral equation (4.2*b*), we have

$$q_0\mathrm{e}^{a\mathrm{i}\theta_0} = \mathrm{e}^{\hat{\mathscr{H}}[\theta_0]}. \tag{5.4}$$

Note that the complex Hilbert transform is applied to θ_0 and integrated over the free surface, where $\theta_0 = O(1)$. Thus $q_0\mathrm{e}^{a\mathrm{i}\theta_0}$ is also of order unity and we conclude from (5.3) that $q_0^3 q_0'$ tends to a constant as $f \to af^*$. Integration then yields the following singular behaviour for q_0,

$$q_0 \sim c_a(f - af^*)^{1/4}. \tag{5.5}$$

In addition, the scaling for $\mathrm{e}^{a\mathrm{i}\theta_0}$ is found from (5.3), giving

$$\mathrm{e}^{a\mathrm{i}\theta_0} \sim \frac{-a\mathrm{i}F_0^2c_a^3}{2}(f - af^*)^{-1/4}. \tag{5.6}$$

Combining these results for q_0 in (5.5) and θ_0 in (5.6) gives the scaling for the complex velocity,

$$\frac{\mathrm{d}f}{\mathrm{d}z} \sim c_a\left(\frac{-a\mathrm{i}F_0^2c_a^3}{2}\right)^{-a}(f - af^*)^{(a+1)/4}. \tag{5.7}$$

Note that $a = 1$ recovers the same singular behaviour of Grant (1973) in the upper-half plane, shown in (5.1).

5.2. *The apparent paradox of a singularity in the lower-half plane*

We see from (5.5) for q_0 that a singularity exists 'within the fluid' in the lower-half plane at $f = -f^*$. This is in contrast to the regular behaviour near the same location provided by Grant's result. Our apparent prediction of singular behaviour in the flow field can readily be resolved by noting that this singularity is for the analytically continued variable, originally relabelled from $q_c \to q$ in § 2.2. It is, thus, important to distinguish between the complexified and 'physical' streamline speeds q_c and q_{phys}, and angles θ_c and θ_{phys}. These physical variables are found by taking the magnitude and argument of the complex velocity $q_0\mathrm{e}^{-\mathrm{i}\theta_0}$ as in (5.7), which is regular for $a = -1$, yielding

$$q_{phys} = \left|q_c\mathrm{e}^{-\mathrm{i}\theta_c}\right| \quad \text{and} \quad \theta_{phys} = \operatorname{Arg}\left(q_c\mathrm{e}^{-\mathrm{i}\theta_c}\right). \tag{5.8a,b}$$

Thus, as $f \to -f^*$ these physical values are regular for the leading-order Stokes wave solution. Only by recombining $q_0\mathrm{e}^{-\mathrm{i}\theta_0}$ to find the physical values within the fluid have these singular terms cancelled out.

https://doi.org/10.1017/jfm.2022.114 Published online by Cambridge University Press

6. Exponential asymptotics

As we show in § 7, the exponentially small ripples are intimately connected with the later term divergence of the asymptotic series (4.1*a*,*b*). In this section, we seek to characterise this divergence.

As we have noted in the previous section, the leading-order solution, q_0 and θ_0, which represents a pure gravity wave, contains singularities at the points $f = af^*$, where $a = \pm 1$ (and further singularities on subsequent Riemann sheets; cf. Crew & Trinh 2016). As later orders depend on successive differentiation of the previous orders, we intuit that as $n \to \infty$, the late terms of q_n and θ_n diverge. In this limit of $n \to \infty$, the divergence can be described by a factorial-over-power ansatz of

$$q_n \sim \frac{Q(f)\Gamma(n+\gamma)}{\chi(f)^{n+\gamma}} \quad \text{and} \quad \theta_n \sim \frac{\Theta(f)\Gamma(n+\gamma)}{\chi(f)^{n+\gamma}}. \tag{6.1a,b}$$

Here, Q, Θ and χ are all functions of f, and γ is assumed to be constant. Note that, more generally, there is a summation of contributions of factorial-over-power type: one for each singularity in $f \in \mathbb{C}$. Typically, the nearest singularities determine the leading-order divergence. As the late terms are determined through a linear perturbative procedure, it is sufficient to consider the general ansatz (6.1*a*,*b*) and add the appropriate contributions once the general forms of Q, Θ and χ are derived.

A consequence of enforcing the $O(B^n)$ energy condition with these solutions is that the Froude number, F_n, is determined as an eigenvalue of the system. Thus, F_n in (4.1*c*) will also diverge in a similar factorial-over-power manner, given by

$$F_n \sim \frac{\delta(n)\Gamma(n+\gamma)}{\Delta^{n+\gamma}}. \tag{6.2}$$

This unusual divergent form arises from satisfying the boundary conditions on the complete solution. The presence of a divergent eigenvalue is a feature typically neglected in similar studies and it will not affect the solvability condition we derive in this work. However, we discuss some subtle considerations of this property in § 9.

The $O(B^n)$ component of Bernoulli's equation (4.4*a*) is a linear differential equation for q_n and θ_n, where terms containing the divergent Froude number, F_n, appear as a forcing term. We solve the homogeneous Bernoulli equation, for which the divergent eigenvalue F_n does not appear. In the discussion of § 9 we provide a more detailed justification of why it is sufficient to neglect the divergent eigenvalue, F_n, and the $O(B^n)$ energy condition. This yields

$$\begin{aligned} &F_0^2\left(q_0^2 q_n' + 2q_0 q_1 q_{n-1}' + 2q_0 q_0' q_n + \cdots\right) + 2F_0 F_1 q_0^2 q_{n-1}' + \cdots \\ &\quad + \theta_n \cos\theta_0 - q_0^2\theta_{n-1}'' - 2q_0 q_1 \theta_{n-2}'' - q_0\theta_0' q_{n-1}' - q_0 q_0' \theta_{n-1}' + \cdots = 0. \end{aligned} \tag{6.3a}$$

In the above equation, we have explicitly written those terms that are necessary to correctly determine the leading- and first-order analysis of the late terms as $n \to \infty$. In particular, note that if the ansatz (6.1*a*,*b*) is differentiated once, then because $(n+\gamma)\Gamma(n+\gamma) = \Gamma(n+\gamma+1)$, the order in n increases by one. Thus, for example, $q_{n-1}' = O(q_n)$ as $n \to \infty$.

Next, we use the boundary-integral equation (4.4*b*) to substitute for θ_n in (6.3*a*). A key idea here, used in previous works on exponential asymptotics and water waves, is that the term that involves the complex Hilbert transform, $\hat{\mathscr{H}}[\theta_n]$, is evaluated on the real axis, and hence away from the singularities $f = af^*$. As a consequence, the

https://doi.org/10.1017/jfm.2022.114 Published online by Cambridge University Press

contribution is exponentially subdominant to the left-hand side of (4.4*b*) as $n \to \infty$. This idea of neglecting $\hat{\mathscr{H}}[\theta_n]$ is a classic step in exponential asymptotics applications of many boundary-integral problems in interfacial flows (cf. § 3 of Chapman (1999), § 5.3 of Trinh, Chapman & Vanden-Broeck (2011) and Trinh (2017)) and can be rigorously justified in such cases (Tanveer & Xie 2003).

With this in mind, we rearrange the boundary-integral equation (4.4*b*) to find

$$\theta_n \sim \frac{a\mathrm{i}q_n}{q_0} - \frac{a\mathrm{i}q_1 q_{n-1}}{q_0^2} + \cdots . \tag{6.3b}$$

From this form, θ''_{n-1}, θ''_{n-2} and θ'_{n-1} are found in terms of q_n and its derivatives. Next, we substitute these into Bernoulli's equation (6.3*a*) and consider the divergent ansatz (6.1*a*,*b*). The leading order in n, which comes from the terms q'_n and q''_{n-1}, is seen to be of order $\Gamma(n+\gamma+1)/\chi^{n+\gamma+1}$. Dividing out by this divergence yields terms that are of $O(1)$, $O(1/n)$, and so on as $n \to \infty$.

Combining (6.3*a*) and (6.3*b*), we obtain at leading order

$$\chi'(q_0 F_0^2 + a\mathrm{i}\chi') = 0. \tag{6.4}$$

We seek the non-trivial function χ that forces the divergence of the asymptotic expansion and, hence, takes the value of $\chi = 0$ at the singularities in f. Assuming that $\chi' \neq 0$, we integrate to find

$$\chi(f) = \chi_a(f) = a\mathrm{i}F_0^2 \int_{af^*}^{f} q_0(f')\,\mathrm{d}f'. \tag{6.5}$$

Here, we have chosen the starting point of integration to be the upper/lower-half singularity at $f = af^*$ where $a = \pm 1$. The function χ, denoted the singulant, plays a pivotal role in the form of the exponentially small terms and the associated Stokes smoothing procedure of § 7. It will be convenient to distinguish between the two singulants using the sub-index a.

At the next order in Bernoulli's equation, $O(1/n)$, we use $\chi' = a\mathrm{i}F_0^2 q_0$ and $\chi'' = a\mathrm{i}F_0^2 q'_0$ to find

$$\frac{Q'}{Q} = 2\frac{q'_0}{q_0} - a\mathrm{i}F_0^2 q_1 - 2a\mathrm{i}F_0 F_1 q_0 + a\mathrm{i}\theta'_0 + \frac{a\mathrm{i}\cos\theta_0}{F_0^2 q_0^3}. \tag{6.6}$$

Thus, by integration, we find

$$Q(f) = Q_a(f) = \Lambda_a q_0^2 \exp\left(a\mathrm{i}\theta_0 + a\mathrm{i}\int_0^f \left[\frac{\cos\theta_0}{F_0^2 q_0^3} - F_0^2 q_1 - 2F_0 F_1 q_0 \right] \mathrm{d}f' \right). \tag{6.7}$$

The starting point of integration has been chosen to be on the free surface at $f = 0$ for convenience. Other points may be chosen, which alters the value of the constant Λ_a. We note that this constant may take different values for $a = 1$ and $a = -1$. Similarly, the form

https://doi.org/10.1017/jfm.2022.114 Published online by Cambridge University Press

of Θ is found using (6.3*b*) and, thus,

$$\Theta(f) = \Theta_a(f) = \frac{aiQ_a(f)}{q_0(f)}. \tag{6.8}$$

Substitution of this solution for $Q(f)$ into ansatz (6.1*a*,*b*) then yields

$$q_n(f) \sim \Lambda_a q_0^2 \exp\left(ai\theta_0 + ai\int_0^f \left[\frac{\cos\theta_0}{F_0^2 q_0^3} - F_0^2 q_1 - 2F_0F_1q_0\right] \mathrm{d}f'\right) \frac{\Gamma(n+\gamma)}{\chi^{n+\gamma}}, \tag{6.9}$$

with χ given by (6.5). A similar form for θ_n may also be found by using the expression for Θ given in (6.8).

6.1. *Determination of γ and Λ*

At this point, we have determined the key components, Q, Θ and χ, that appear in the factorial-over-power ansatz (6.1*a*,*b*). This leaves the value of the constants γ and Λ_a. Note that our asymptotic series (4.1*a*,*b*) reorders as $f \to af^*$ (for which $q_0 = O(Bq_1)$ for instance) and the matched asymptotics procedure that results in investigating this limit yields γ and Λ_a.

In order to determine the constant γ, we take the limit $f \to af^*$ and match the order of the singularity of the divergent ansatz, valid for n large, to the low-order behaviour. Setting $n = 0$ in (6.9) and taking the limit of $f \to af^*$ yields

$$q_n|_{n=0} = O\left(\frac{q_0^2}{\chi^\gamma} \exp\left(ai\theta_0 + ai\int_0^f \left[\frac{\cos\theta_0}{F_0^2 q_0^3} - F_0^2 q_1 - 2F_0F_1q_0\right] \mathrm{d}f'\right)\right). \tag{6.10}$$

From the scalings of q_0 and θ_0 in § 5.1, and the scaling of q_1 in Appendix A we find that

$$\left.\begin{aligned} \chi^\gamma &= O((f-af^*)^{5\gamma/4}), \\ q_0^2 \exp\left(ai\int_0^f \left[\frac{\cos\theta_0}{F_0^2 q_0^3} - F_0^2 q_1 - 2F_0F_1q_0\right] \mathrm{d}f\right) &= O\left((f-af^*)^{5/4}\right). \end{aligned}\right\} \tag{6.11}$$

We substitute the above into (6.10) and match to $q_0 = O(f-af^*)^{1/4}$ to find

$$\gamma = \tfrac{4}{5}. \tag{6.12}$$

As is the case in many exponential asymptotic analyses, the determination of the constant prefactor, Λ_a, is often the most troublesome aspect of the procedure. For our purposes, it will be sufficient to know that Λ_a is a non-zero constant, and can be determined via the solution of a numerical recursion relation. Specifically, it is found by matching the 'inner' limit of q_n from the divergent form (6.9) with the 'outer' limit of the inner solution for q near $f = af^*$. This analysis is performed in Appendix B, yielding

$$\Lambda_a = -\frac{2if^*}{F_0^2 c_a^4} \mathrm{e}^{-\mathcal{P}(af^*)} \left(\frac{4aiF_0^2c_a}{5}\right)^{4/5} \lim_{n\to\infty} \frac{\hat{q}_n}{\Gamma(n+\gamma)}. \tag{6.13}$$

Here, $\hat{q}_n$ is the nth term of the outer limit of an inner solution holding near $f = af^*$, and can be determined by recurrence relation (B14). The constant c_a is the prefactor of the singular scaling of q_0 from (5.6) whereas $\mathcal{P}(af^*)$ is given in (A7). We do not need to work with the precise value of Λ_a; however, later in §§ 6.2 and 7.3, the fact that Λ_1 and Λ_{-1} are

https://doi.org/10.1017/jfm.2022.114 Published online by Cambridge University Press

complex conjugates will be crucial to obtain a real-valued solution on the free surface. As the prefactor, Λ_a, only has a scaling effect on the solutions (and is independent of B), it will be convenient to choose a specific value for visualisation purposes in § 8.

6.2. *The divergence along the free surface*

In order to capture the divergence of q_n along the free surface, $\mathrm{Im}[f] = 0$, we must include the effects of the two symmetrically placed crest singularities indexed by $a = \pm 1$. We thus write

$$\mathfrak{q}_n = q_n|_{a=1} + q_n|_{a=-1}. \tag{6.14}$$

By the results of § B.3, the constants Λ_1 and Λ_{-1} are the complex conjugates of one another. With regards to the two singulants, χ_1 and χ_{-1}, we may split the path of integration via

$$\chi_a(\phi) = a\mathrm{i}F_0^2\left[\int_{af^*}^{0} + \int_0^{\phi}\right] q_0(f')\,\mathrm{d}f', \tag{6.15}$$

for $f = \phi$ along the real axis. As q_0 takes real values on the free-surface, $\mathrm{Im}[f] = 0$, the second integral above is seen to take purely imaginary values. By the Schwarz reflection principle, q_0 evaluated on the imaginary axis between $-af^*$ and af^* is purely real and symmetric about the origin. Therefore the first integral on the right-hand side of (6.15) is purely real and takes the same value regardless of the choice of a. Thus, χ_{-1} and χ_1 are also the complex conjugates of one another on the free surface.

Due to this behaviour of Λ_a and χ_a, we write

$$\Lambda_a = |\Lambda_1|\exp[a\mathrm{i}\arg\Lambda_1] \quad \text{and} \quad \chi_a(\phi) = |\chi_1(\phi)|\exp[a\mathrm{i}\arg\chi_1(\phi)], \tag{6.16a,b}$$

which upon substitution into $\mathfrak{q}_n = q_n|_{a=1} + q_n|_{a=-1}$ yields

$$\mathfrak{q}_n(\phi) = \frac{2|\Lambda_1|q_0^2\Gamma(n+\gamma)}{|\chi_1(\phi)|^{n+\gamma}}\cos\left[\arg\Lambda_1 - (n+\gamma)\arg\chi_1(\phi) + \theta_0 + I(\phi)\right], \tag{6.17}$$

where we have defined

$$I(\phi) = \int_0^{\phi}\left(\frac{\cos\theta_0}{F_0^2q_0^3} - F_0^2q_1 - 2F_0F_1q_0\right)\mathrm{d}\phi'. \tag{6.18}$$

Thus, the above form (6.17) captures the real-valued divergence on the free-surface.

We have successfully derived an expression for the late term divergence on the axis in (6.17) and off the axis in (6.9).

7. Stokes line smoothing

One of the key ideas of exponential asymptotics is that there exists a link between the factorial-over-power form of the divergences, given (6.1*a*,*b*) and (6.17), and the exponentially small terms we wish to derive. Following the work of Dingle (1973), Stokes lines are contours in the f-plane for which both

$$\mathrm{Im}[\chi_a(f)] = 0 \quad \text{and} \quad \mathrm{Re}[\chi_a(f)] \geqslant 0. \tag{7.1a,b}$$

Across and in the vicinity of these contours, exponentially small terms in the solution smoothly change in magnitude across a boundary layer. This is known as the

https://doi.org/10.1017/jfm.2022.114 Published online by Cambridge University Press

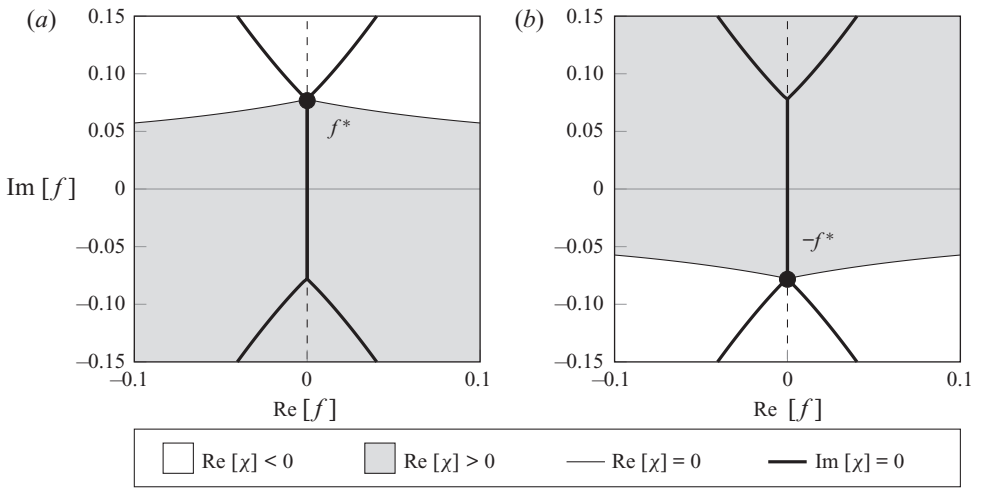


Figure 7. Values of the singulant, χ_a, are shown from the upper-half singularity in (*a*), with $a = 1$, and from the lower-half singularity in (*b*), with $a = -1$. The Stokes lines, which satisfy conditions (7.1*a*,*b*), are shown by the thick lines in the grey-shaded regions. This configuration corresponds to the energy $\mathscr{E} = 0.3804$ for which the upper-half plane singularity is at $f^* \approx 0.07776\mathrm{i}$. The chosen branch cuts for each of these singularities are shown by dashed lines.

Stokes phenomenon. In this section, we discuss the configuration of Stokes lines, and then perform the optimal truncation and Stokes-line-smoothing procedures needed to derive the exponentially small capillary ripples.

7.1. *Analysis of the Stokes lines*

To find the Stokes lines for our problem, we apply conditions (7.1*a*,*b*) to our expression for the singulant, χ_a, given in (6.5) as

$$\chi_a(f) = a\mathrm{i}F_0^2 \int_{af^*}^{f} q_0(f')\,\mathrm{d}f'. \tag{7.2}$$

Here, integration begins at the principal singularity, $f' = af^*$, that lies in the analytic continuation of the free surface. Note that unlike many traditional studies in exponential asymptotics, the determination of the singulant function requires the leading-order solution, q_0, for which there does not exist a closed-form analytical solution. We use numerical values of q_0 to evaluate the singulant, χ_a.

The procedure is as follows. Given a fixed value of the energy, we obtain numerical values of q_0 and θ_0 along the free-surface $\mathrm{Im}[f] = 0$ using the numerical computations of Shelton *et al.* (2021) or any standard procedure for calculating gravity Stokes waves (cf. Vanden-Broeck 1986). Next, the analytic continuation method of Crew & Trinh (2016) is used to find q_0 and θ_0 in the complex f-plane. Values for χ_a are then found across the domain by integrating q_0 along paths originating at either singularity. Graphs of the critical contours of $\mathrm{Im}[\chi_a]$ and $\mathrm{Re}[\chi_a]$ are given in figure 7 for the two choices of $a = 1$ and $a = -1$. We see that there are two Stokes lines along the imaginary axis from $f = -f^*$ to $f = f^*$, one for $a = 1$ and another for $a = -1$, which intersect with the free surface at the wave crest $\phi = 0$.

Note that only the Stokes lines that intersect with the free-surface, $\mathrm{Im}[f] = 0$, are considered; other Stokes lines would indicate a switching on or switching off of

https://doi.org/10.1017/jfm.2022.114 Published online by Cambridge University Press

exponentials in the general complex plane, but are not associated with the physical production of surface ripples.

7.2. *Optimal truncation*

In order to capture the exponentially small components of the solution, which do not appear in the Poincaré series (4.1*a*,*b*), we truncate the series at $n = N - 1$ by considering

$$q = \underbrace{\sum_{n=0}^{N-1} B^n q_n}_{q_r} + \bar{q}, \quad \theta = \underbrace{\sum_{n=0}^{N-1} B^n \theta_n}_{\theta_r} + \bar{\theta} \quad \text{and} \quad F = \underbrace{\sum_{n=0}^{N-1} B^n F_n}_{F_r} + \bar{F}, \tag{7.3a–c}$$

and, thus, we have introduced the notation of q_r, θ_r and F_r for the truncated regular expansions of the solutions and eigenvalue.

We demonstrate that when truncated optimally at the point where two consecutive terms are of the same order, that is, choose N such that $|B^N q_N| \sim |B^{N+1} q_{N+1}|$, the remainders $\bar{q}$, $\bar{\theta}$ and $\bar{F}$ will be exponentially small. This point of optimal truncation is given by

$$N = \frac{|\chi_a|}{B} + \rho, \tag{7.4}$$

where $\rho \in [0, 1)$ is a bounded number to ensure N is an integer.

Substituting these into the boundary-integral equation (2.9*b*) yields a relationship between $\bar{\theta}$ and $\bar{q}$, given by

$$\bar{\theta} = \frac{a\mathrm{i}\bar{q}}{q_r} - a\mathrm{i}\xi_{int} - a\mathrm{i}\hat{\mathscr{H}}[\bar{\theta}] + O(\bar{q}^2). \tag{7.5}$$

Similarly we can insert the truncations (7.3*a–c*) into Bernoulli's equation (2.9*a*). This gives a second-order differential equation for $\bar{q}$ and $\bar{\theta}$. Upon substituting for $\bar{\theta}$ from (7.5), this is reduced down to an equation for $\bar{q}$ only. Furthermore, we neglect the Hilbert transform of the remainder, $\hat{\mathscr{H}}[\bar{\theta}]$, as this is anticipated to be exponentially subdominant. This yields

$$\begin{aligned}
&\left[a\mathrm{i}Bq_r\right]\bar{q}'' + \left[-F_r^2 q_r^2 - a\mathrm{i}Bq_r' + Bq_r\theta_r' - a\mathrm{i}Bq_r\xi_{int}'\right]\bar{q}' \\
&\quad + \left[-\frac{a\mathrm{i}\cos\theta_r}{q_r} - 2F_r^2 q_r q_r' + \frac{a\mathrm{i}B(q_r')^2}{q_r} + Bq_r'\theta_r'\right. \\
&\quad \left. - a\mathrm{i}Bq_r'' + 2Bq_r\theta_r'' - a\mathrm{i}Bq_r'\xi_{int}' - 2a\mathrm{i}Bq_r\xi_{int}''\right]\bar{q} - 2F_r q_r^2 q_r'\bar{F} = \mathcal{R} + O(\bar{q}^2).
\end{aligned} \tag{7.6}$$

This is a second-order differential equation for $\bar{q}$, in which the forcing terms on the right-hand side are of $O(B^N)$. A similar equation was derived by Trinh (2017) for the low-Froude limit of gravity waves. Here, we have introduced the forcing terms ξ_{int} and ξ_{bern} arising from the Poincaré expansion in the boundary-integral and Bernoulli's equations as

$$\xi_{int} = \hat{\mathscr{H}}[\theta_r] - a\mathrm{i}\theta_r - \log q_r, \tag{7.7a}$$

$$\xi_{bern} = F_r^2 q_r^2 q_r' + \sin(\theta_r) - B(q_r^2\theta_r'' + \theta_r' q_r' q_r), \tag{7.7b}$$

$$\mathcal{R} = \xi_{bern} - a\mathrm{i}\cos\theta_r\xi_{int} + a\mathrm{i}Bq_r q_r'\xi_{int}' + a\mathrm{i}Bq_r^2\xi_{int}''. \tag{7.7c}$$

Due to the truncation at $n = N - 1$, equation (7.6) is satisfied exactly for every order up to and including B^{N-1} because $\xi_{int} = O(B^N)$ and $\xi_{bern} = O(B^N)$.

https://doi.org/10.1017/jfm.2022.114 Published online by Cambridge University Press

7.3. *Stokes line smoothing*

We now seek a closed-form asymptotic expression for $\bar{q}$ and the terms switched-on across Stokes lines. We start with the homogeneous form of (7.6), in which the terms on the right-hand side and $\bar{F}$ are neglected. Following the exponential asymptotics methodology established in, e.g., § 4 of Chapman & Vanden-Broeck (2006), we note that the homogeneous problem has solutions of the form,

$$\bar{q}_{homog} \sim Q_a(f) \exp\left(-\frac{\chi_a(f)}{B}\right), \tag{7.8}$$

where $\chi_a(f)$ and $Q_a(f)$ satisfy those same equations as found for the late-term ansatz via (6.4) and (6.6). To observe the Stokes phenomenon and the switching of exponentials, we now include the forcing terms on the right-hand side of (7.6) for $\bar{q}$. We consider a solution of the form

$$\bar{q}(f) = A_a(f) Q_a(f) \exp\left(-\frac{\chi_a(f)}{B}\right), \tag{7.9}$$

where the Stokes multiplier $A_a(f)$ is introduced to capture the switching behaviour that occurs across the Stokes lines. When the truncation point, N, is chosen optimally as in (7.4), $\bar{q}$ will be seen to be exponentially small and will change in magnitude across the lines where $\mathrm{Im}[\chi_a] = 0$ and $\mathrm{Re}[\chi_a] \geqslant 0$.

The algebra for this procedure follows very similarly to, e.g., Chapman *et al.* (1998), Chapman & Vanden-Broeck (2006) and Trinh (2017). Thus, when the exponential form of (7.9) for $\bar{q}$ is substituted into (7.6), the dominant balance at leading order is identically satisfied by our choice of χ determined in (6.4). The first non-trivial balance occurs at $O(\mathrm{e}^{-\chi/B})$, which also involves the forcing terms on the right-hand side. We extract the $O(B^N)$ terms from $\mathcal{R}$ in (7.7*c*), and this yields $\mathcal{R} \sim -q_0^2 \theta''_{N-1} B^N$. The governing equation for A_a is then given by

$$\left[F_0^2 q_0^2 Q_a \mathrm{e}^{-\chi_a/B}\right] \frac{\mathrm{d}A_a}{\mathrm{d}f} \sim -a\mathrm{i} q_0 q''_{N-1} B^N, \tag{7.10}$$

where we have used $\theta''_{N-1} \sim a\mathrm{i} q_0^{-1} q''_{N-1}$ from the boundary-integral equation (6.3*b*).

By substituting in the factorial-over-power form for q''_{N-1} from (6.1*a*,*b*), and using the chain rule to change differentiation to be in terms of χ_a, we find

$$\frac{\mathrm{d}A_a}{\mathrm{d}\chi_a} = \frac{B^N \mathrm{e}^{\chi_a/B} \Gamma(N+1+\gamma)}{\chi_a^{N+1+\gamma}}. \tag{7.11}$$

This is now of an equivalent form to that found by Chapman & Vanden-Broeck (2006) for the low-Froude limit of gravity waves (cf. their (4.4)). In brief, the procedure is as follows. First, we write $\chi_a = r_a \mathrm{e}^{\mathrm{i}\vartheta_a}$ and truncate optimally via (7.4) with $N = r_a/B + \rho$. Examination of the differential equation (7.11) shows that there exists a boundary layer at $\vartheta_a = 0$ and indeed this is the anticipated Stokes line where $\mathrm{Im}[\chi_a] = 0$. The appropriate inner variable near the Stokes line is $\vartheta_a = B^{1/2}\overline{\vartheta}_a$ and (7.11) can then be integrated to show

$$A_a(f) = C_a + \frac{\sqrt{2\pi}\mathrm{i}}{B^\gamma} \int_{-\infty}^{\overline{\vartheta}_a \sqrt{r_a}} \exp\left(-t^2/2\right) \mathrm{d}t, \tag{7.12}$$

where C_a is constant. Taking the outer limit of $\overline{\vartheta} \to \infty$, we then see that across the Stokes line, there is a jump of

$$A_a(\vartheta_a \to 0-) - A_a(\vartheta_a \to 0+) = \frac{2\pi\mathrm{i}}{B^\gamma}. \tag{7.13}$$

https://doi.org/10.1017/jfm.2022.114 Published online by Cambridge University Press

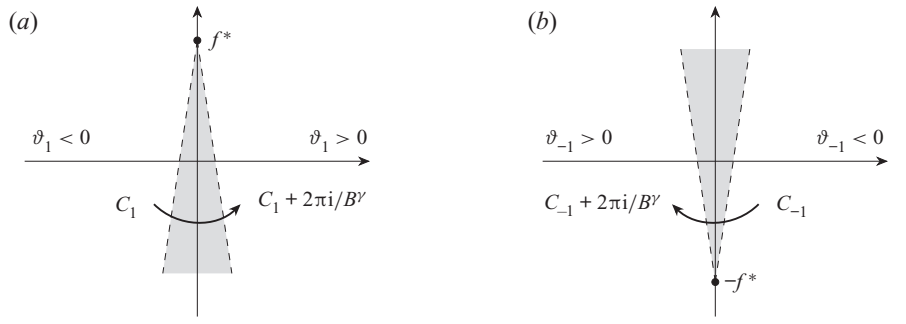


Figure 8. The Stokes smoothing procedure is visualised in the f-plane for (*a*) $a = 1$ and (*b*) $a = -1$.

As concerns the relationship between Stokes-line contributions from $f = f^*$ and $f = -f^*$, note that as χ_1 is the complex conjugate of χ_{-1}, we have $\vartheta_1 = -\vartheta_{-1}$. Thus, we anticipate that C_1 switches to $C_1 + 2\pi\mathrm{i}/B^\gamma$ as one proceeds from left-to-right across the Stokes line from $f = f^*$. This is shown in figure 8(*a*). On the other hand, C_{-1} switches to $C_{-1} + 2\pi\mathrm{i}/B^\gamma$ proceeding from right-to-left across the Stokes line from $f = -f^*$. This is shown in figure 8(*b*). We emphasise that the above Stokes smoothing procedure only provides the local change of the prefactor, A_a, across the Stokes line. Determination of the constant, C_a, will follow from imposition of the boundary conditions.

Returning now to (7.9), we write the leading-order exponentials on the axis, $\mathrm{Im}[f] = 0$, via $\bar{\mathfrak{q}} = \bar{q}|_{a=1} + \bar{q}|_{a=-1}$, either as an inner solution

$$\bar{\mathfrak{q}}(\phi) = A_1(\phi)Q_1(\phi)\exp\left(-\frac{\chi_1(\phi)}{B}\right) + A_{-1}(\phi)Q_{-1}(\phi)\exp\left(-\frac{\chi_{-1}(\phi)}{B}\right), \tag{7.14a}$$

for which $A(\phi)$ is given by (7.12), or as an outer solution by

$$\bar{\mathfrak{q}}(\phi) \sim \begin{cases} C_1\left(Q_a\mathrm{e}^{-\chi_a/B}\right)\big|_{a=1} + \left\{C_{-1} + \dfrac{2\pi\mathrm{i}}{B^\gamma}\right\}\left(Q_a\mathrm{e}^{-\chi_a/B}\right)\big|_{a=-1} & \text{for } \phi < 0, \\ \left\{C_1 + \dfrac{2\pi\mathrm{i}}{B^\gamma}\right\}\left(Q_a\mathrm{e}^{-\chi_a/B}\right)\big|_{a=1} + C_{-1}\left(Q_a\mathrm{e}^{-\chi_a/B}\right)\big|_{a=-1} & \text{for } \phi > 0. \end{cases} \tag{7.14b}$$

In (7.14*b*), the constants, C_1 and C_{-1}, will be determined by enforcing periodicity on $\bar{\mathfrak{q}}$ and $\bar{\mathfrak{q}}'$, as given by

$$\bar{\mathfrak{q}}\left(-\tfrac{1}{2}\right) = \bar{\mathfrak{q}}\left(\tfrac{1}{2}\right) \quad \text{and} \quad \bar{\mathfrak{q}}'\left(-\tfrac{1}{2}\right) = \bar{\mathfrak{q}}'\left(\tfrac{1}{2}\right). \tag{7.15a,b}$$

The second relation above arose by evaluating the derivative of periodicity condition (2.4*b*) at $\phi = 0$. In writing $C_1 = C_1^R + \mathrm{i}C_1^I$ and $C_{-1} = C_{-1}^R + \mathrm{i}C_{-1}^I$, we have four unknowns balancing the four equations from the real and imaginary parts of (7.15*a*,*b*). Using $\Lambda_a = |\Lambda_1|\mathrm{e}^{a\mathrm{i}\arg\Lambda_1}$ from (6.16*a*,*b*) and $\chi_a = \mathrm{Re}[\chi_1] + a\mathrm{i}\,\mathrm{Im}[\chi_1]$ then yields the solutions

$$\left.\begin{aligned} C_1^I &= -\frac{\pi}{B^\gamma}, \quad C_1^R = -\frac{\pi}{B^\gamma}\frac{\cos\left[G(1/2)\right]}{\sin\left[G(1/2)\right]}, \\ C_{-1}^I &= -\frac{\pi}{B^\gamma}, \quad C_{-1}^R = -\frac{\pi}{B^\gamma}\frac{\cos\left[G(1/2)\right]}{\sin\left[G(1/2)\right]}, \end{aligned}\right\} \tag{7.16}$$

where

$$G(\phi) = \theta_0(\phi) + \int_0^\phi \left[\frac{\cos\theta_0}{F_0^2 q_0^3} - F_0^2 q_1 - 2F_0F_1q_0 - \frac{F_0^2 q_0}{B}\right]\mathrm{d}\phi. \tag{7.17}$$

https://doi.org/10.1017/jfm.2022.114 Published online by Cambridge University Press

Solutions are not possible when $\sin[G(1/2)] = 0$, from which we obtain the following discrete set of values of B,

$$B_n = \frac{F_0^2 \displaystyle\int_0^{1/2} q_0 \,\mathrm{d}\phi}{\theta_0(1/2) + \displaystyle\int_0^{1/2} \left[\frac{\cos\theta_0}{F_0^2 q_0^3} - F_0^2 q_1 - 2F_0 F_1 q_0 \right] \mathrm{d}\phi + n\pi} \quad \text{for } n \in \mathbb{Z}^+. \tag{7.18}$$

Formula (7.18) provides the crucial eigenvalue condition for the non-existence of solutions. Recall that the 'parameters' in this formula, e.g. $\{F_0, F_1, q_0, q_1, \theta_0\}$, are dependent on the chosen energy, $\mathscr{E}$, in (2.9*c*). Note that $\theta_0(1/2) = 0$ and, in addition, only solutions with positive integer values of n correspond to positive values of the Bond number. Thus, for instance, it is predicted that solutions do not exist at a countably infinite set of discrete values,

$$B_1(\mathscr{E}) > B_2(\mathscr{E}) > B_3(\mathscr{E}) > \cdots > B_n(\mathscr{E}) > \cdots > 0. \tag{7.19}$$

In the next section, we show that these values of B are associated with points between adjacent 'fingers' of solutions in the bifurcation diagram.

Substitution of (7.16) for C_1 and C_{-1} into (7.14*b*) then gives a real-valued solution on the free surface. First, for $\phi < 0$, we have

$$\bar{\mathfrak{q}}(\phi) = -\frac{2\pi}{B^\gamma} |\Lambda_1| q_0^2 \mathrm{e}^{-\mathrm{Re}[\chi_1]/B} \left[\frac{\cos(G(1/2))}{\sin(G(1/2))} \cos[\arg \Lambda_1 + G(\phi)] - \sin[\arg \Lambda_1 + G(\phi)] \right], \tag{7.20a}$$

whereas for values on the positive real axis $\phi > 0$,

$$\bar{\mathfrak{q}}(\phi) = -\frac{2\pi}{B^\gamma} |\Lambda_1| q_0^2 \mathrm{e}^{-\mathrm{Re}[\chi_1]/B} \left[\frac{\cos(G(1/2))}{\sin(G(1/2))} \cos[\arg \Lambda_1 + G(\phi)] + \sin[\arg \Lambda_1 + G(\phi)] \right]. \tag{7.20b}$$

Note that the above forms for $\bar{\mathfrak{q}}$ are valid away from the boundary layer surrounding the Stokes line at $\phi = 0$.

8. Numerical comparisons with the full water-wave model

We now compare the asymptotic results of § 7.3 with the numerical solutions of the fully nonlinear equations (2.1*a*)–(2.1*d*) found by Shelton *et al.* (2021). These numerical solutions were calculated using a spectral method on a domain, ϕ, uniformly discretised with $N = 1024$ points (cf. § 4 of Shelton *et al.* (2021) for details).

8.1. *Finding values for our analytical solution*

To obtain precise values for our analytical solution, $\bar{\mathfrak{q}}$, across the domain, we use the form given in (7.14*a*). This form includes the local change across the boundary layer at $\phi = 0$ and requires known values of q_0, θ_0, F_0, q_1 and F_1 for a specified value of the energy, $\mathscr{E}$.

In order to calculate values for these nonlinear solutions, we employ Newton iteration on the $O(1)$ and $O(B)$ (4.2) and (4.3) with an even discretisation of the domain, ϕ. With these values known, the three components of $\bar{\mathfrak{q}}$, the Stokes prefactor, $A_a(\phi)$, the functional prefactor, $Q_a(\phi)$, and the singulant, $\chi_a(\phi)$, may then be calculated individually with a specified value of B.

https://doi.org/10.1017/jfm.2022.114 Published online by Cambridge University Press

(i) For $Q_a(\phi)$ given in (6.7), we take the previously computed values for θ_0, q_0, F_0, q_1 and F_1 and employ numerical integration across the domain. As noted in § 6.1, it is convenient to choose a value of $|\Lambda_a|$ in order to facilitate visualisation of the ripples. In figures 9 and 11, we plot $\bar{\mathbf{q}}$ with $|\Lambda_a| = 1$. In figure 10, in order to compare between asymptotic and numerical solutions, we have chosen $|\Lambda_a| = 0.006$, which is estimated by numerical fitting. It can be verified that fitting to other fingers changes the constant by only a small amount.

(ii) To determine $\chi_a(\phi)$, we split the range of integration as in (6.15). This allows for $\mathrm{Re}[\chi_a]$ to be calculated by integrating q_0 through the complex-valued domain from the singularity at $f = af^*$ to the wave crest at $f = 0$. Next, $\mathrm{Im}[\chi_a]$ is found by integrating q_0 over the free surface from $f = 0$ to $f = \phi$. Values for the integrand, q_0, are found with the analytic continuation method from Crew & Trinh (2016) described in § 7.1.

(iii) To find the Stokes prefactor, $A_a(\phi)$, from (7.12), the upper limit of the integral is determined by using $r_a = |\chi_a|$ and $\bar{\vartheta} = \arg \chi_a/B$ from the known values of χ_a. The integral is then calculated with known values of the error function. The constants C_a are then found by calculating $G(1/2)$ from (7.17).

This process yields values for our exponentially small component of the solution, $\bar{\mathbf{q}}$, for specified values of B and $\mathscr{E}$. The values of B_n where the solvability condition fails from (7.18) are also found with the same method used for Q_a above.

8.2. *Comparisons*

We begin by comparing the values of B_n (where the solvability condition fails) with the (B, F) bifurcation space computed numerically by Shelton *et al.* (2021). In taking the same value of the energy, $\mathscr{E} = 0.3804$, we visualise these points in the (B, F)-plane by approximating F_n by $F_n \approx F_0 + B_n F_1$ (an error of $O(B^2)$). This comparison is shown in figure 9. These locations where perturbation solutions are non-existent show excellent agreement with the points between adjacent branches of solutions where numerical solutions could not be calculated.

In addition, four of our analytical solution profiles, $\bar{\mathbf{q}}$, are shown in insets (a)–(d) of this figure. These solutions have been selected to lie in the midpoint of the solution branch, with a Bond number of $(B = (B_n + B_{n+1})/2)$. They demonstrate that the ripples obtain their greatest magnitude at the edge of the periodic domain. Note that these ripples are plotted on a zero background state. These same solutions are also shown in figure 10, which includes the first two terms of the asymptotic expansion, $q_0 + Bq_1$. These have been provided to compare the magnitude of the ripples in relation to the leading-order Stokes wave.

In our previous numerical work, we demonstrated that as one of the solution branches was transversed, the solution develops an extra wavelength, and this was seen to occur near the top of the solution branch. We observe that the same effect occurs with our analytical solutions. This is demonstrated in figure 11, in which we provide eight solution profiles equally spaced in the Bond number between two adjacent values of B_n. From these, we see that as we travel from right to left across the solution branch by decreasing the value of B, an additional ripple forms in the centre of the domain.

https://doi.org/10.1017/jfm.2022.114 Published online by Cambridge University Press

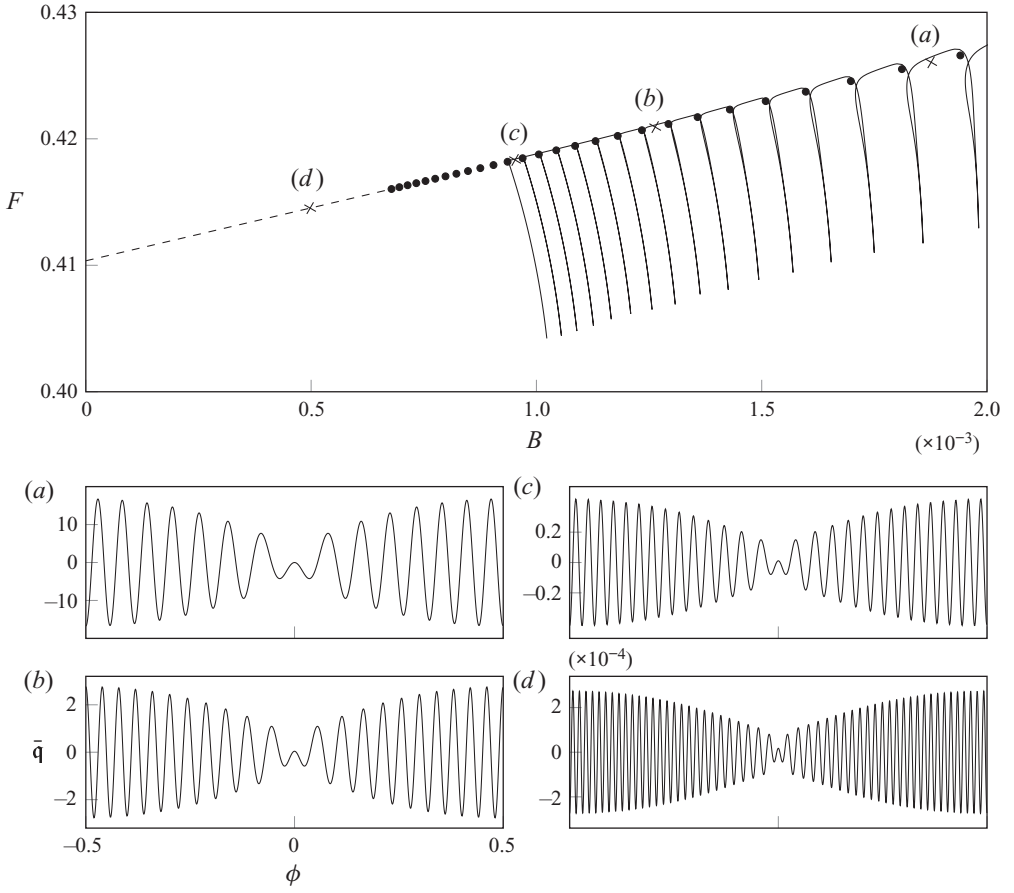


Figure 9. A comparison between the numerical solution branches of Shelton *et al.* (2021) (shown solid) and the analytical approximations of B_n from (7.18) (shown as black circles). Insets (*a*)–(*d*) show the exponentially small ripples, $\bar{\mathrm{q}}$, from (7.20) for the four locations of $B = 0.001876$, $B = 0.001264$, $B = 0.0009527$ and $B = 0.0004978$ (shown as crosses in the main inset). The solutions are all computed at $\mathscr{E} = 0.3804$. A value of $|A_a| = 1$ has been used for the constant prefactor.

8.3. *The effects of changing the energy, $\mathscr{E}$*

All of the above solutions have been computed for the same fixed value of the energy, $\mathscr{E} = 0.3804$. We now relax this restriction by considering values of $\mathscr{E}$ between 0 and 0.9. Note that the limiting Stokes wave is not the most energetic (cf. § 6 of Longuet-Higgins & Fox 1978) and for values of $\mathscr{E}$ very close to unity, there are multiple possible solutions beyond the classical Stokes wave. We do not consider solutions too close to the highest wave ($\mathscr{E} > 0.9$) in this work.

In figure 12 we show how the locations where the solvability condition fails, $B_n(\mathscr{E})$, change with the energy for values of $n \leqslant 40$. We note that as the energy deceases to zero and we enter the linear regime, these lines tend towards the predictions by Wilton (1915). These are the discrete values of the Bond number for which two linear solutions of wavenumbers 1 and n also have the same Froude number. Thus, a single leading-order gravity wave of the type assumed in this work is insufficient for describing Wilton's linear solutions, and is why we recover his values under this limit.

https://doi.org/10.1017/jfm.2022.114 Published online by Cambridge University Press

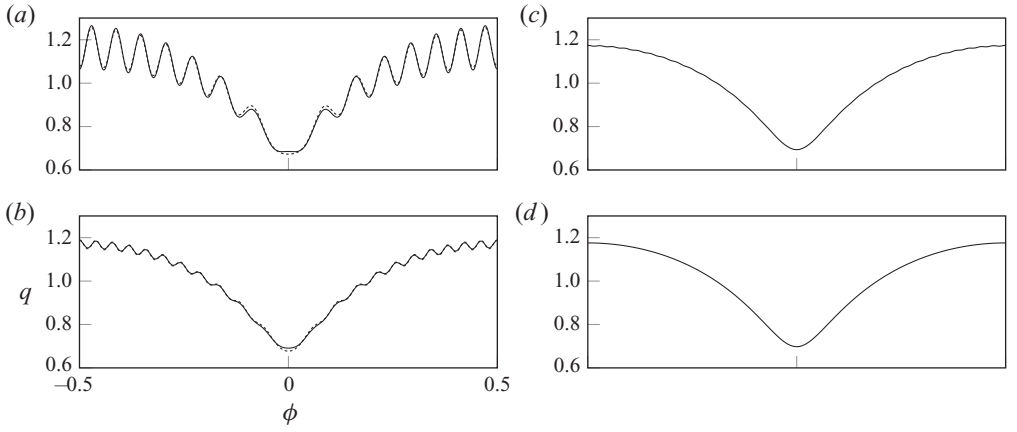


Figure 10. The analytical solution, $q = q_0 + Bq_1 + \bar{q}$, is shown (line) for the four profiles calculated in figure 9. For comparison, numerical solutions with the same value of B and $\mathscr{E}$ are shown dashed in insets (a) and (b). A value of $|\Lambda_a| = 0.006$ has been used for these comparisons, estimated from numerical comparisons.

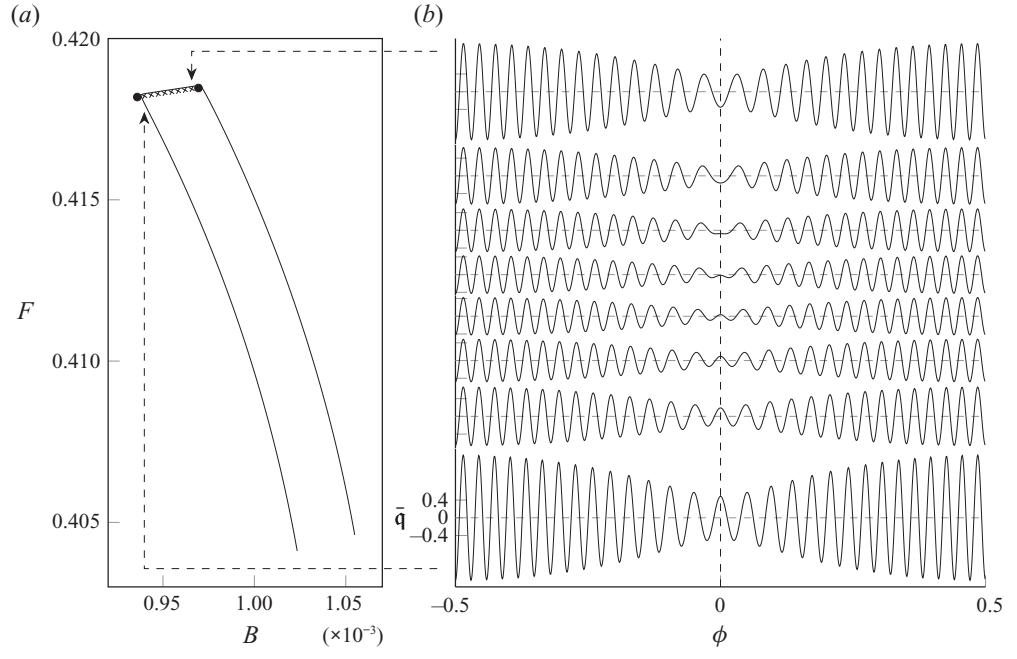


Figure 11. Here, for $\mathscr{E} = 0.3804$, we plot the exponentially small solution, $\bar{\mathfrak{q}}$, from (7.20) between the two values of $B_{29} = 0.0009360$ and $B_{28} = 0.0009694$. Note that the base gravity wave is thus not shown. The eight chosen values of B (crosses) are equally spaced between the values of B_{29} and B_{28}. This corresponds to the finger $G_{28\to29}$ found numerically by Shelton *et al.* (2021). A value of $|\Lambda_a| = 1$ has been used for the constant prefactor.

We have also chosen to provide values of $\mathrm{Re}[\chi]$ for different values of $\mathscr{E}$, as this controls the exponential behaviour of the magnitude of our parasitic ripples. This is shown in figure 13, and shows that the constant controlling the exponential behaviour of our solution increases with the energy, $\mathscr{E}$.

https://doi.org/10.1017/jfm.2022.114 Published online by Cambridge University Press

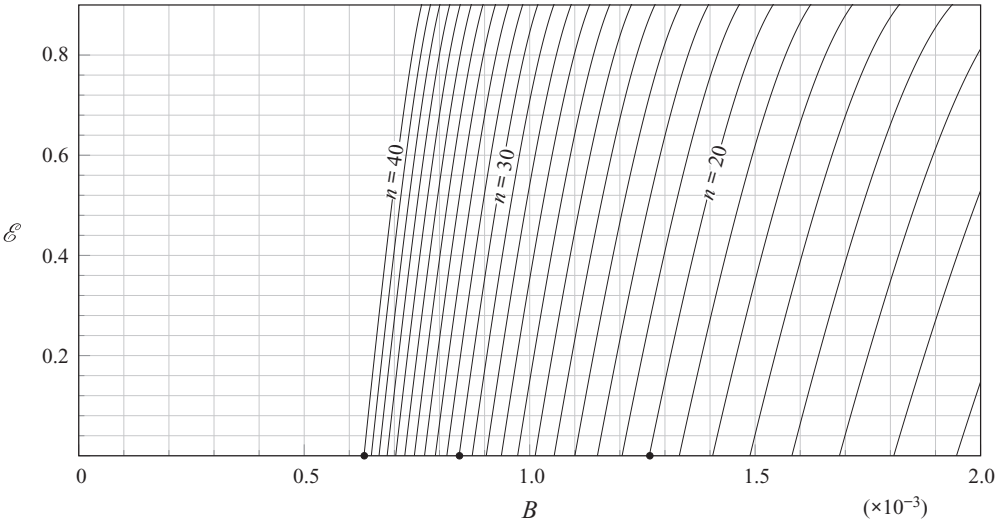


Figure 12. Values for B_n, where the solvability condition fails, are shown for different values of the energy, $\mathscr{E}$. The small-$\mathscr{E}$ predictions by Wilton (1915) are shown by the black dots at $\mathscr{E} = 0$ for $n = 20$, 30 and 40.

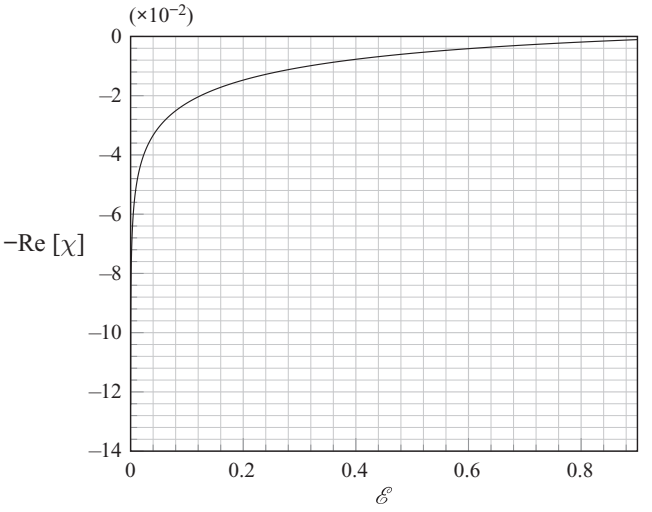


Figure 13. The value of $-\mathrm{Re}[\chi]$ from (6.15) is shown for different values of the energy, $\mathscr{E}$.

9. Discussion

9.1. *Open and resolved challenges in exponential asymptotics*

Over the past 20 years, the application of exponential asymptotics to fluid mechanical problems has been very successful in the discovery and development of new analytical methodologies (Boyd 1998). However, there are a number of distinguishing features in our treatment of the parasitic ripples problem that are particularly interesting.

First, the majority of preceding works in exponential asymptotics typically rely upon the derivation of a crucial singulant function, χ, for which an exact analytical form is known. In our analysis, however, the singulant in (6.5) requires the complex integration of a nonlinear gravity wave, which must be precomputed. Moreover, the values of χ and the

https://doi.org/10.1017/jfm.2022.114 Published online by Cambridge University Press

associated Stokes lines must be determined in the complex plane, and this has necessitated a separate study of the distribution and properties of the singularities of the Stokes wave problem (Crew & Trinh 2016) as a precursor to the present work.

Second, there are a number of challenging steps in the exponential asymptotics analysis that we highlight here. The reader should note two interesting features.

(i) The eigenvalues, F_n, are divergent, but we have not had to rely upon their form in the derivation of $\mathfrak{q}_n$ in § 6.
(ii) Our factorial-over-power expression for $\mathfrak{q}_n$, valid only in the limit $n \to \infty$, satisfies neither the energy condition nor the periodicity conditions on q_n and q_n'. This is because our approximation of this divergence is only valid in the vicinity of the Stokes line about which the Stokes phenomenon occurs, rather than globally.

Through a more detailed analysis, it is possible to derive both a factorial-over-power ansatz for F_n, as well as the additional terms necessary so that the late-term approximation satisfies the energetic and periodicity conditions. We provide a brief comment on the procedure, but some of these issues are more easily observed in a simpler eigenvalue problem exhibiting divergence; this will be the focus of future work by the current authors (authors' unpublished observations).

In essence, the eigenvalue divergence produces inhomogeneous contributions to Bernoulli's equation depending on F_n, F_{n-1}, ... (compare (6.3*a*) with (4.4*a*)). These contributions, of the form (6.2), will force additional components in the late-term representation of the solution. Both the periodicity and energy constraints can then be satisfied with the inclusion of further components associated with $\chi' = 0$, currently neglected following (6.4). Once these additional divergences are included, a prediction for the eigenvalue, F_n, is obtained.

As it turns out, however, these additional components are subdominant to the divergent ansatz (6.1*a*,*b*) with $\chi = \chi_a(f)$ given by (6.5) near the relevant Stokes lines. Consequently, these components will not influence the Stokes smoothing procedure derived in § 7. We note that this is analogous to how the complex Hilbert transform, $\hat{\mathscr{H}}[\theta_n]$, is neglected in the discussion following (6.3*a*).

9.2. *Asymmetry in steady and temporal water-waves*

It is important to note that in this work, following Longuet-Higgins (1963), we have focused on a fairly restricted view of parasitic ripples that correspond to the classical potential flow formulation of a steadily travelling wave composed of a perturbation about a symmetric nonlinear gravity wave. This assumption also follows from the class of solutions first detected by Shelton *et al.* (2021).

We would expect that within this steady potential framework, it is possible to obtain general asymmetric gravity–capillary solutions exhibiting small-scale ripples in the $B \to 0$ limit. Indeed, solutions resembling this anticipated structure have been calculated by previous authors; for instance Zufiria (1987*b*) considered symmetry breaking in gravity–capillary waves for moderately small values of the surface-tension coefficient. The properties of the waves in that study match those presented in this paper, as some appear to be perturbations about the asymmetric gravity waves found in Zufiria (1987*a*). The general detection of asymmetric gravity–capillary waves remains a challenging problem (cf. Gao, Wang & Vanden-Broeck 2017).

However, it is likely that the above relaxation of symmetry in the solutions does not lead to the typical distribution of asymmetric capillary ripples that appear on the forward

https://doi.org/10.1017/jfm.2022.114 Published online by Cambridge University Press

face of a steep travelling wave. In order to produce the asymmetry viewed in experimental results, it is likely necessary to consider further modifications to this theory (cf. Perlin & Schultz 2000). Possible extensions include accounting for the additional effects of time dependence, viscosity or vorticity.

The problem of time-dependent parasitic waves has been studied numerically by multiple authors, such as Hung & Tsai (2009), Murashige & Choi (2017) and Wilkening & Zhao (2021). For instance, Hung & Tsai (2009) studied a time-dependent formulation that includes vortical effects; a pure gravity wave is chosen as the initial condition and time-evolution results in the formation of parasitic ripples ahead of the wave crest. Similar methodologies have been implemented by, e.g., Deike, Popinet & Melville (2015) in order to study the formation of time-dependent parasitic ripples in the full Navier–Stokes system using a volume-of-fluid method. We note that small-scale ripples can also occur near the crest of gravity waves as they approach a limiting formulation, as shown by Chandler & Graham (1993) for solutions close to the steady Stokes wave of extreme form and Mailybaev & Nachbin (2019) for finite-depth breaking waves. In our present work, the authors are examining the application of exponential asymptotic techniques to the description of time-dependent parasitic ripples. The inclusion of time dependence in asymptotics beyond-all-orders remains a poorly understood problem, and very few authors including Chapman & Mortimer (2005), Lustri (2013) and Lustri, Pethiyagoda & Chapman (2019), have considered such a complication.

Analogously, the extension of models of gravity–capillary waves to include non-zero viscosity, vorticity or finite depth have been considered by various authors. For instance Longuet-Higgins (1963, 1995) and Fedorov & Melville (1998) considered viscous gravity–capillary waves which exhibit asymmetry. Furthermore, we would expect that a similar application of exponential asymptotics to the case of periodic finite-depth flows could be achieved; in the shallow-water limit, the results would match those presented in seminal works on generalised solitary waves in Kortewe–de Vries equations (see e.g. Yang & Akylas (1996, 1997) and chapter 10 of Boyd 1998). It is an interesting question to consider the equivalent exponential asymptotic analysis for these more complex problems where we expect similar phenomena to arise.

10. Conclusions

We have considered the small surface-tension limit of gravity–capillary waves of infinite depth. This results in gravity-wave solutions at leading order. The parasitic ripples, which have a wavelength much smaller than that of the base gravity wave, appear beyond all orders of the asymptotic expansion as their amplitude is exponentially small in the Bond number. The analytical solution for these from (7.20) has been found by

(i) observing the divergence of the Poincaré series $q = q_0 + Bq_1 + \ldots$, a consequence of singularities in the analytic continuation of the leading-order solution, q_0;
(ii) optimally truncating the divergent expansion at $N \sim 1/B$ and considering the exponentially small remainder $\bar{q}$ by a solution of the form $q = q_0 + Bq_1 + \cdots + B^N q_N + \bar{q}$;
(iii) identifying the Stokes lines (which depend on q_0) and calculating the effect of Stokes phenomenon on the exponentially small terms.

We have also found a solvability condition for our problem, which fails at discrete values of the Bond number given by (7.18). These points were shown in figure 9 to coincide with

https://doi.org/10.1017/jfm.2022.114 Published online by Cambridge University Press

the discrete nature of the numerical solution branches. Moreover, we have demonstrated that if the leading-order gravity wave is taken to be symmetric, these parasitic ripples must also exhibit symmetry about the wave crest; presenting a fundamental improvement in our understanding of the structure of these parasitic waves.

Our results provide an analytical theory and framework for the numerical solutions detected in Shelton *et al.* (2021). Moreover, we have shown that, although certain details of Longuet-Higgins (1963) theory of parasitic capillary ripples are correct, an exponential asymptotics approach provides verifiable asymptotic predictions, corrected functional relationships, and connection of the ripples to Stokes lines and the Stokes phenomenon.

Acknowledgements. We thank Professors P. Milewski and J. Toland (Bath) for helpful discussions, and the anonymous reviewers for their insightful comments on our work.

Funding. This work was supported by the Engineering and Physical Sciences Research Council (EP/V012479/1).

Declaration of interests. The authors report no conflict of interest.

Author ORCIDs.
Josh Shelton https://orcid.org/0000-0001-6257-5190;
Philippe H. Trinh https://orcid.org/0000-0003-3227-1844.

Appendix A. Singular scaling of the order B quantities

In § 6.1, the inner limit of q_n as $f \to af^*$ relied on the singular behaviour of the $O(B)$ term q_1. Taking the $O(B)$ equations, we substitute θ_1 from the boundary-integral equation (4.3*b*) into Bernoulli's equation (4.3*a*) to find

$$F_0^2 q_0^2 \frac{\mathrm{d}q_1}{\mathrm{d}f} + \left[2F_0^2 q_0 q_0' + \frac{a\mathrm{i}\cos\theta_0}{q_0}\right] q_1 + 2F_0 F_1 q_0^2 q_0' - a\mathrm{i}\hat{\mathscr{H}}[\theta_1]\cos\theta_0 - q_0(q_0\theta_0')' = 0. \tag{A1}$$

The singular scaling of $\cos\theta_0$ can be found from (5.6) to be

$$\cos\theta_0 \sim \frac{1}{2}\mathrm{e}^{a\mathrm{i}\theta_0} \sim \frac{-a\mathrm{i}F_0^2 c_a^3}{4}(f - af^*)^{-1/4}. \tag{A2}$$

Thus, the term involving the complex-valued Hilbert transform $\hat{\mathscr{H}}[\theta_1]$, which acts on the free surface upon which $\theta_1 \sim O(1)$, is subdominant in (A1). The same is true for the term containing $2F_0F_1q_0^2q_0'$. The singular scaling of the four remaining dominant terms in (A1) can then be found by the results of § 5.1, yielding

$$\left.\begin{aligned} &F_0^2 q_0^2 \frac{\mathrm{d}q_1}{\mathrm{d}f} \sim F_0^2 c_a^2 (f - af^*)^{1/2}\frac{\mathrm{d}q_1}{\mathrm{d}f}, \quad 2F_0^2 q_0 q_0' q_1 \sim \frac{F_0^2 c_a^2}{2}(f - af^*)^{-1/2} q_1, \\ &\frac{a\mathrm{i}\cos\theta_0}{q_0} q_1 \sim \frac{F_0^2 c_a^2}{4}(f - af^*)^{-1/2} q_1, \quad -q_0(q_0\theta_0')' \sim \frac{3a\mathrm{i}c_a^2}{16}(f - af^*)^{-3/2}. \end{aligned}\right\} \tag{A3}$$

In substituting the ansatz $q_1 \sim A(f - af^*)^n$ into (A1), we then find

$$q_1 \sim \frac{3a\mathrm{i}}{4F_0^2}(f - af^*)^{-1}. \tag{A4}$$

https://doi.org/10.1017/jfm.2022.114 Published online by Cambridge University Press

A.1. *Inner limit of $Q_a(f)$*

To determine the value of the constant Λ_a, the analysis of which is performed in Appendix B, we require the inner limit of the prefactor, $Q_a(f)$, of the naive solution. Taking $Q_a(f)$ from (6.7), we consider the singular behaviour of q_0 and $\mathrm{e}^{ai\theta_0}$ from (5.5) and (5.6) to find

$$Q_a(f) \sim \frac{-\Lambda_a a\mathrm{i}F_0^2c_a^5}{2}(f-af^*)^{1/4} \times \exp\left(\int_0^f a\mathrm{i}\left[\frac{\cos\theta_0}{F_0^2q_0^3} - F_0^2q_1 - 2F_0F_1q_0\right]\mathrm{d}f\right) \quad \text{as } f \to af^*. \tag{A5}$$

It remains to evaluate the integral in the above equation as $f \to af^*$. In considering the singular behaviour of the integrand, we find

$$a\mathrm{i}\left[\frac{\cos\theta_0}{F_0^2q_0^3} - F_0^2q_1 - 2F_0F_1q_0\right] \sim (f-af^*)^{-1} + O(1). \tag{A6}$$

In writing

$$\mathcal{P}(f) = \int_0^f a\mathrm{i}\left[\frac{\cos\theta_0}{F_0^2q_0^3} - F_0^2q_1 - 2F_0F_1q_0\right] - (f-af^*)^{-1}\,\mathrm{d}f, \tag{A7}$$

and noting that $q_1 \sim 3a\mathrm{i}/4F_0^2(f-af^*)^{-1} + O(1)$, we see that $\mathcal{P}(f) \sim O(1)$ as $f \to af^*$. This formulation yields

$$\int_0^f a\mathrm{i}\left[\frac{\cos\theta_0}{F_0^2q_0^3} - F_0^2q_1 - 2F_0F_1q_0\right]\mathrm{d}f = \mathcal{P}(f) + \log(f-af^*) - \log(-af^*), \tag{A8}$$

from which we find the singular behaviour of $Q_a(f)$ to be

$$Q_a(f) \sim \frac{\Lambda_a\mathrm{i}F_0^2c_a^5}{2f^*}\mathrm{e}^{\mathcal{P}(af^*)}(f-af^*)^{5/4} \quad \text{as } f \to af^*. \tag{A9}$$

Appendix B. An inner solution at the principal singularities

The constant Λ_a appearing in the prefactor of q_n in (6.9) is determined by matching the inner limit of q_n with the outer limit of a solution holding near the singularity at $f = af^*$. In the inner region near this point, Bernoulli's equation (2.9*a*) holds,

$$F^2q^2\frac{\mathrm{d}q}{\mathrm{d}f} + \frac{1}{2\mathrm{i}}(\mathrm{e}^{\mathrm{i}\theta} - \mathrm{e}^{-\mathrm{i}\theta}) - Bq\frac{\mathrm{d}}{\mathrm{d}f}\left(q\frac{\mathrm{d}\theta}{\mathrm{d}f}\right) = 0. \tag{B1}$$

We also have the boundary-integral equation (2.9*b*) applying in this inner region. As the complex-valued Hilbert transform $\hat{\mathscr{H}}[\theta]$ appearing in the right-hand side of this operates on values of θ from the free surface in the outer region, away from the singularity, we can use the outer expansion in powers of B. At each order in B, $\hat{\mathscr{H}}[\theta_n]$ is then related to the outer solutions of q_n and θ_n by evaluating the boundary-integral equation at this order.

https://doi.org/10.1017/jfm.2022.114 Published online by Cambridge University Press

This gives

$$\begin{aligned}\log(q) + a\mathrm{i}\theta &= \hat{\mathscr{H}}[\theta] \\ &= \hat{\mathscr{H}}[\theta_0] + B\hat{\mathscr{H}}[\theta_1] + O(B^2) \\ &= (\log q_0 + a\mathrm{i}\theta_0) + B(q_1/q_0 + a\mathrm{i}\theta_1) + O(B^2). \end{aligned} \tag{B2}$$

To evaluate this in the inner region, we take the inner limit of $f \to af^*$ on the right-hand side. Exponentiating (B2) and using the scaling of q_0 and $\mathrm{e}^{a\mathrm{i}\theta_0}$ from (5.5) and (5.6) gives

$$q\mathrm{e}^{a\mathrm{i}\theta} \sim -\frac{a\mathrm{i}F_0^2c^4}{2} + O(B). \tag{B3}$$

From this, we find at leading order both $\mathrm{e}^{\mathrm{i}\theta} - \mathrm{e}^{-\mathrm{i}\theta} = 2q/(\mathrm{i}F_0^2c^4) - (\mathrm{i}F_0^2c^4)/2q$ and $q\theta' = a\mathrm{i}q'$. Substituting these into Bernoulli's equation (B1) then gives the inner equation

$$F^2q^2\frac{\mathrm{d}q}{\mathrm{d}f} - \frac{q}{F_0^2c^4} - \frac{F_0^2c^4}{4q} - a\mathrm{i}Bq\frac{\mathrm{d}^2q}{\mathrm{d}f^2} = 0. \tag{B4}$$

B.1. *Boundary layer scalings*

The width of the boundary layer at the principal upper- and lower-half plane singularities is determined by the reordering of the outer expansion $q_{outer} = q_0 + Bq_1 + O(B^2)$ when consecutive terms become comparable. Balancing $q_0 \sim Bq_1$ for simplicity, where $q_0 \sim c_a(f - af^*)^{1/4}$ from (5.5) and $q_1 \sim 3a\mathrm{i}/4F_0^2(f - af^*)^{-1}$ from (A4), we find the width of the boundary layer to be $B^{4/5}$. Thus, we introduce the inner variable η by

$$(f - af^*) = B^{4/5}\eta. \tag{B5}$$

In addition, in the inner region $\bar{q}_{inner} \sim q_0$. By incorporating the inner variable η with our scaling for q_0, we have $q_0 \sim c_a(f - af^*)^{1/4} \sim c_aB^{1/5}\eta^{1/4}$. This tells us how to rescale q_{outer} to produce an $O(1)$ quantity, $\bar{q}_{inner}$, in the inner region, given by

$$q_{outer} = c_aB^{1/5}\eta^{1/4}\bar{q}_{inner}. \tag{B6}$$

To find the outer limit of $\bar{q}_{inner}$, we consider a series expansion as $\eta \to \infty$. The form of this series is determined by substituting the inner limit of the expansion for q_{outer} into (B6), giving

$$\begin{aligned} q_{outer} = \sum_{n=0}^{\infty} B^nq_n &\sim \sum_{n=0}^{\infty} \frac{B^nQ_a\Gamma(n+\gamma)}{\chi_a^{n+\gamma}} \\ &\sim \sum_{n=0}^{\infty} \frac{\mathrm{i}\Lambda_aB^nF_0^2c_a^5\,\mathrm{e}^{\mathcal{P}(af^*)}(f - af^*)^{5/4}\Gamma(n+\gamma)}{2f^*\left[\dfrac{4a\mathrm{i}F_0^2c_a}{5}(f - af^*)^{5/4}\right]^{n+\gamma}} \\ &\sim \sum_{n=0}^{\infty} \frac{\mathrm{i}\Lambda_aB^{1/5}F_0^2c_a^5\,\mathrm{e}^{\mathcal{P}(af^*)}\Gamma(n+\gamma)\eta^{1/4}}{2f^*\left(\dfrac{4a\mathrm{i}F_0^2c_a}{5}\eta^{5/4}\right)^n\left(\dfrac{4a\mathrm{i}F_0^2c_a}{5}\right)^{4/5}}. \end{aligned} \tag{B7}$$

Here, we have used $\chi_a \sim 4a\mathrm{i}F_0^2c_a/5(f - af^*)^{5/4}$, $\gamma = 4/5$, the singular behaviour of Q_a from (A9) and the inner variable η introduced in (B5). In denoting the constant prefactor

https://doi.org/10.1017/jfm.2022.114 Published online by Cambridge University Press

of χ_a to be $X = 4aiF_0^2 c_a/5$, we find by (B6) the expected series form for $\bar{q}_{inner}$,

$$\bar{q}_{inner} \sim \sum_{n=0}^{\infty} \frac{\mathrm{i}\Lambda_a F_0^2 c_a^4 \, \mathrm{e}^{\mathcal{P}(af^*)} \Gamma(n+\gamma)}{2f^*(X\eta^{5/4})^n X^{4/5}}. \tag{B8}$$

This suggests that in taking

$$z = X\eta^{5/4}, \tag{B9}$$

the anticipated series for $\bar{q}_{inner}$ will be of the form

$$\bar{q}_{inner} = \sum_{n=0}^{\infty} \frac{\hat{q}_n}{z^n}. \tag{B10}$$

B.2. *Inner expansion*

Substituting both the inner variable η from (B5), and $\bar{q}_{inner}$ from (B6) into the governing equation for the inner region (B4) gives

$$c_a F_0^2 \bar{q}^3 \left(\eta \frac{\mathrm{d}\bar{q}}{\mathrm{d}\eta} + \frac{\bar{q}}{4}\right) - \frac{ai\bar{q}^2}{\eta^{5/4}} \left(\eta^2 \frac{\mathrm{d}^2\bar{q}}{\mathrm{d}\eta^2} + \frac{\eta}{2}\frac{\mathrm{d}\bar{q}}{\mathrm{d}\eta} - \frac{3\bar{q}}{16}\right) = \frac{c_a F_0^2}{4}. \tag{B11}$$

Using the substitution $z = 4aiF_0^2 c_a \eta^{5/4}/5$ presented in (B9) results in a more convenient expansion in integer powers of $1/z$. With this, (B11) becomes

$$\bar{q}^3 \left(5z\frac{\mathrm{d}\bar{q}}{\mathrm{d}z} + \bar{q}\right) + \frac{\bar{q}^2}{z}\left(5z^2\frac{\mathrm{d}^2\bar{q}}{\mathrm{d}z^2} + 3z\frac{\mathrm{d}\bar{q}}{\mathrm{d}z} - \frac{3\bar{q}}{5}\right) = 1. \tag{B12}$$

The outer limit of the inner solution to this equation as $z \to \infty$ is considered by the series (B10). Substituting this into the inner equation (B12) yields at leading order

$$\hat{q}_0^4 = 1. \tag{B13}$$

By considering the $O(z^{-n})$ term in (B12), the following recurrence relation is found for $\hat{q}_n$,

$$\begin{aligned}
&(5n-4)\hat{q}_0^3\hat{q}_n \\
&\quad = \sum_{k=1}^{n-1} \hat{q}_{n-k}\left[\hat{q}_0^2\hat{q}_k + \sum_{p=1}^{k}\hat{q}_{k-p}\left(\frac{(5p-6)(5p-2)}{5}\hat{q}_{p-1} + \sum_{j=0}^{p}(1-5j)\hat{q}_j\hat{q}_{p-j}\right)\right] \\
&\qquad + \hat{q}_0\sum_{p=1}^{n-1}\hat{q}_{n-p}\left(\frac{(5p-6)(5p-2)}{5}\hat{q}_{p-1} + \sum_{j=0}^{p}(1-5j)\hat{q}_j\hat{q}_{p-j}\right) \\
&\qquad + \frac{(5n-6)(5n-2)}{5}\hat{q}_0^2\hat{q}_{n-1} + \hat{q}_0^2\sum_{j=1}^{n-1}(1-5j)\hat{q}_j\hat{q}_{n-j}.
\end{aligned} \tag{B14}$$

https://doi.org/10.1017/jfm.2022.114 Published online by Cambridge University Press

B.3. *Determining the constant* Λ_a

In comparing the nth term of $\bar{q}_{inner}$ between representations (B8) and (B10), we find the following expression for the constant Λ_a:

$$\Lambda_a = \frac{-2\mathrm{i}f^*}{F_0^2 c_a^4}\mathrm{e}^{-\mathcal{P}(af^*)}\left(\frac{4aiF_0^2c_a}{5}\right)^{4/5}\lim_{n\to\infty}\frac{\hat{q}_n}{\Gamma(n+\gamma)}. \tag{B15}$$

By applying Schwartz reflection principle to q_0, which is real valued on the free surface, $\mathrm{Im}[f] = 0$, we see that $c_{a=1}$ and $c_{a=-1}$ are the complex conjugates of one another.

The recurrence relation (B14) may then be solved numerically and yields $\lim_{n\to\infty}\hat{q}_n/\Gamma(n+\gamma) \approx 1.4\times10^{-3}$. Once the secondary components of (B15) are computed, this gives a numerical value for Λ_a.

References

Berry, M.V. 1989 Uniform asymptotic smoothing of Stokes's discontinuities. *Proc. R. Soc. Lond.* A **422** (1862), 7–21.

Boyd, J.P. 1998 *Weakly Nonlocal Solitary Waves and Beyond-All-Orders Asymptotics*. Kluwer Academic.

Chandler, G.A. & Graham, I.G. 1993 The computation of water waves modelled by Nekrasov's equation. *SIAM J. Numer. Anal.* **30** (4), 1041–1065.

Chapman, S.J. 1999 On the role of Stokes lines in the selection of Saffman–Taylor fingers with small surface tension. *Eur. J. Appl. Maths* **10** (6), 513–534.

Chapman, S.J., King, J.R. & Adams, K.L. 1998 Exponential asymptotics and Stokes lines in nonlinear ordinary differential equations. *Proc. R. Soc. Lond.* A **454**, 2733–2755.

Chapman, S.J. & Mortimer, D.B. 2005 Exponential asymptotics and Stokes lines in a partial differential equation. *Proc. R. Soc. Lond.* A **461** (2060), 2385–2421.

Chapman, S.J. & Vanden-Broeck, J.-M. 2006 Exponential asymptotics and gravity waves. *J. Fluid Mech.* **567**, 299–326.

Crapper, G.D. 1957 An exact solution for progressive capillary waves of arbitrary amplitude. *J. Fluid Mech.* **2** (6), 532–540.

Crew, S.C. & Trinh, P.H. 2016 New singularities for Stokes waves. *J. Fluid Mech.* **798**, 256–283.

Deike, L., Popinet, S. & Melville, W.K. 2015 Capillary effects on wave breaking. *J. Fluid Mech.* **769**, 541–569.

Dingle, R.B. 1973 *Asymptotic Expansions: Their Derivation and Interpretation*. Academic.

Fedorov, A.V. & Melville, W.K. 1998 Nonlinear gravity–capillary waves with forcing and dissipation. *J. Fluid Mech.* **354**, 1–42.

Gao, T., Wang, Z. & Vanden-Broeck, J.-M. 2017 Investigation of symmetry breaking in periodic gravity–capillary waves. *J. Fluid Mech.* **811**, 622–641.

Grant, M.A. 1973 The singularity at the crest of a finite amplitude progressive Stokes wave. *J. Fluid Mech.* **59** (2), 257–262.

Hung, L.-P. & Tsai, W.-T. 2009 The formation of parasitic capillary ripples on gravity–capillary waves and the underlying vortical structures. *J. Phys. Oceanogr.* **39** (2), 263–289.

Longuet-Higgins, M.S. 1963 The generation of capillary waves by steep gravity waves. *J. Fluid Mech.* **16**, 138–159.

Longuet-Higgins, M.S. 1995 Parasitic capillary waves: a direct calculation. *J. Fluid Mech.* **301**, 79–107.

Longuet-Higgins, M.S. & Fox, M.J.H. 1977 Theory of the almost-highest wave: the inner solution. *J. Fluid Mech.* **80** (04), 721–741.

Longuet-Higgins, M.S. & Fox, M.J.H. 1978 Theory of the almost-highest wave. Part 2. Matching and analytic extension. *J. Fluid Mech.* **85** (04), 769–786.

Lustri, C.J., Pethiyagoda, R. & Chapman, S.J. 2019 Three-dimensional capillary waves due to a submerged source with small surface tension. *J. Fluid Mech.* **863**, 670–701.

Lustri, C.J. 2013 Exponential asymptotics in unsteady and three-dimensional flows. PhD thesis, Oxford University.

Mailybaev, A.A. & Nachbin, A. 2019 Explosive ripple instability due to incipient wave breaking. *J. Fluid Mech.* **863**, 876–892.

Murashige, S. & Choi, W. 2017 A numerical study on parasitic capillary waves using unsteady conformal mapping. *J. Comput. Phys.* **328**, 234–257.

https://doi.org/10.1017/jfm.2022.114 Published online by Cambridge University Press

OLDE DAALHUIS, A.B., CHAPMAN, S.J., KING, J.R., OCKENDON, J.R. & TEW, R.H. 1995 Stokes phenomenon and matched asymptotic expansions. *SIAM J. Appl. Maths* **55** (6), 1469–1483.

PERLIN, M., LIN, H. & TING, C.-L. 1993 On parasitic capillary waves generated by steep gravity waves: an experimental investigation with spatial and temporal measurements. *J. Fluid Mech.* **255**, 597–620.

PERLIN, M. & SCHULTZ, W.W. 2000 Capillary effects on surface waves. *Annu. Rev. Fluid Mech.* **32** (1), 241–274.

SHELTON, J., MILEWSKI, P. & TRINH, P.H. 2021 On the structure of steady parasitic gravity–capillary waves in the small surface tension limit. *J. Fluid Mech.* **922**, A16.

TANVEER, S. & XIE, X. 2003 Analyticity and nonexistence of classical steady Hele-Shaw fingers. *Commun. Pure Appl. Maths* **56** (3), 353–402.

TRINH, P.H. 2017 On reduced models for gravity waves generated by moving bodies. *J. Fluid Mech.* **813**, 824–859.

TRINH, P.H., CHAPMAN, S.J. & VANDEN-BROECK, J.-M. 2011 Do waveless ships exist? Results for single-cornered hulls. *J. Fluid Mech.* **685**, 413–439.

VANDEN-BROECK, J.-M. 1986 Steep gravity waves: Havelock's method revisited. *Phys. Fluids* **29** (9), 3084–3085.

VANDEN-BROECK, J.-M. 2010 *Gravity-Capillary Free-Surface Flows*. Cambridge University Press.

WILKENING, J. & ZHAO, X. 2021 Quasi-periodic travelling gravity–capillary waves. *J. Fluid Mech.* **915**, A7.

WILTON, J.R. 1915 On ripples. *Phil. Mag.* **29** (173), 688–700.

YANG, T.-S. & AKYLAS, T.R. 1996 Weakly nonlocal gravity–capillary solitary waves. *Phys. Fluids* **8** (6), 1506–1514.

YANG, T.-S. & AKYLAS, T.R. 1997 On asymmetric gravity–capillary solitary waves. *J. Fluid Mech.* **330**, 215–232.

ZUFIRIA, J.A. 1987*a* Non-symmetric gravity waves on water of infinite depth. *J. Fluid Mech.* **181**, 17–39.

ZUFIRIA, J.A. 1987*b* Symmetry breaking in periodic and solitary gravity–capillary waves on water of finite depth. *J. Fluid Mech.* **184**, 183–206.

https://doi.org/10.1017/jfm.2022.114 Published online by Cambridge University Press